

Iron and Chromium Complexes Containing Tridentate Chelates Based on Nacnac and Imino- and Methyl-Pyridine Components: Triggering C—X Bond Formation

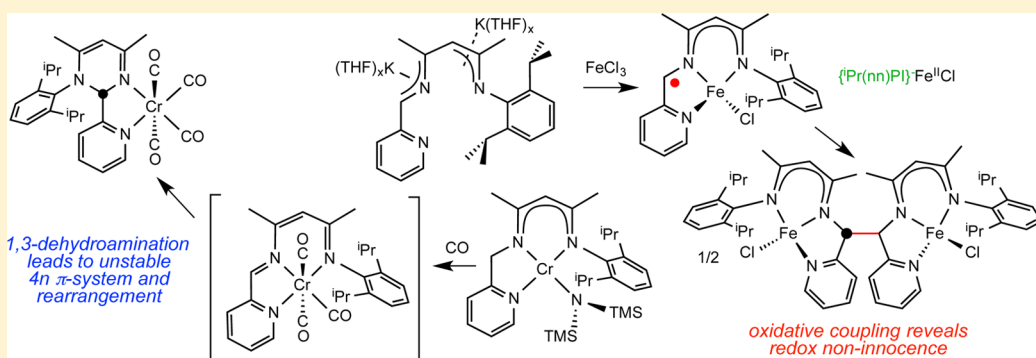
Wesley D. Morris,[†] Peter T. Wolczanski,^{*,†} Jörg Sutter,[‡] Karsten Meyer,[‡] Thomas R. Cundari,[§] and Emil B. Lobkovsky[†]

[†]Department of Chemistry & Chemical Biology, Baker Laboratory, Cornell University, Ithaca, New York 14853, United States

[‡]Department of Chemistry & Pharmacy, University of Erlangen-Nuremberg, Egerlandstr. 1, D-91058 Erlangen, Germany

[§]Department of Chemistry, Center for Advanced Scientific Computing and Modeling (CASCaM), University of North Texas, Box 305070, Denton, Texas 76203-5070, United States

Supporting Information



ABSTRACT: Nacnac-based tridentate ligands containing a pyridyl-methyl and a 2,6-dialkyl-phenylamine (i.e., $(2,6\text{-R}_2\text{C}_6\text{H}_3\text{N}=\text{C}(\text{Me})\text{CH}=\text{C}(\text{Me})\text{NH}(\text{CH}_2\text{py})$; $\text{R} = \text{Et}$, $\{\text{Et}(\text{nn})\text{PM}\}\text{H}$; $\text{R} = ^i\text{Pr}$, $\{^i\text{Pr}(\text{nn})\text{PM}\}\text{H}$) were synthesized by condensation routes. Treatment of $\text{M}\{\text{N}(\text{TMS})_2\}\text{THF}_n$ ($\text{M} = \text{Cr}$, $n = 2$; $\text{M} = \text{Fe}, \text{Co}$, $n = 1$; TMS = trimethylsilane; THF = tetrahydrofuran) with $\{^i\text{Pr}(\text{nn})\text{PM}\}\text{H}$ afforded $\{^i\text{Pr}(\text{nn})\text{PM}\}\text{M}(\text{TMS})_2$ (**1-M^{iPr}**; $\text{M} = \text{Cr}, \text{Fe}$); $\{\text{Et}(\text{nn})\text{PM}\}\text{M}(\text{TMS})_2$ (**1-Et^{iPr}**; $\text{M} = \text{Fe}, \text{Co}$) was similarly obtained. $\{\text{R}(\text{nn})\text{PM}\}\text{FeBr}$ ($\text{R} = ^i\text{Pr}$, Et ; 2-Fe^R) were prepared from FeBr_2 and $\{\text{R}(\text{nn})\text{PM}\}\text{Li}$, and alkylated to generate $\{\text{R}(\text{nn})\text{PM}\}\text{Fe}^\text{neoPe}$ ($\text{R} = ^i\text{Pr}$, Et ; 3-Fe^R). Carbonylation of 3-Fe^R provided $\{^i\text{Pr}(\text{nn})\text{PM}\}\text{Fe}(\text{CO}^\text{neoPe})\text{CO}$ (**4-Fe^{iPr}**), and carbonylations of **1-Fe^R** ($\text{R} = \text{Et}$, ^iPr) and **1-Cr^{iPr}** induced deamination to afford $\{\text{R}(\text{nn})\text{PI}\}\text{Fe}(\text{CO})_2$ ($\text{R} = ^i\text{Pr}$, **5-Fe^{iPr}**, Et , **5-Fe^{Et}**), where PI is pyridine-imine, and $\{\kappa^2\text{-N,N-pyrim-pyr}\}\text{Cr}(\text{CO})_4$ (**6-Cr^{iPr}**), in which the aryl-amide side of the nacnac attacked the incipient PI group. Carbon–carbon bonds were formed at the imine carbon of the $\{\text{R}(\text{nn})\text{PI}\}$ ligand. Addition of $\{[{}^i\text{Pr}(\text{nn})\text{PI}]^{2-}\}(\text{K}^+(\text{THF})_x)_2$ to FeCl_3 generated $\{^i\text{Pr}(\text{nn})\text{CHPy}\}_2\text{Fe}_2\text{Cl}_2$ (**7-Fe^{iPr}**), and TMSN_3 induced the deamination of **1-Fe^{Et}**, but with disproportionation to provide $\{[\text{Et}(\text{nn})\text{CHPy}]_2\}\text{Fe}$ (**8-Fe^{Et}**). Ph_2CN_2 induced C–C bond formation with **1-Fe^{iPr}** via its thermal degradation to ultimately afford $\{^i\text{Pr}(\text{nn})\text{CHPy}\}_2(\text{FeN}=\text{CPh}_2)_2$ (**9-Fe^{iPr}**). The compounds were examined by X-ray crystallography (**1-M^{iPr}**, $\text{M} = \text{Cr}, \text{Fe}$; **1-Co^{Et}**; **2-Fe^{iPr}**; **4-Fe^{iPr}**; **5-Fe^{iPr}**; **6-Cr^{iPr}**; **7-Fe^{iPr}**; **8-Fe^{Et}**; **9-Fe^{iPr}**), Mössbauer spectroscopy, and NMR spectroscopy. Structural parameters assessing redox noninnocence are discussed, as are structural and mechanistic consequences of the various electronic environments.

1. INTRODUCTION

Ligands that are precursors to or contain the 2-azaallyl functionality^{1–6} were examined in the context of carbon–carbon bond formation, and mixed results were achieved. A number of compounds containing smif (smif = di-2-pyridyl-2-azaallyl) and its variants have manifested C–C bond formation reactivity (Figure 1).^{3–5} For example, the monomer (smif)- $\text{FeN}(\text{TMS})_2$ (TMS = trimethylsilane) crystallizes out of solution as the dimer $[(\text{smif})\text{FeN}(\text{TMS})_2]_2$ (**A**), which contains two C–C bonds, and *ortho*-methylation of smif renders a diiron complex with a single new C–C bond and

pyridine-imine radical anion components (**B**).³ *In situ* deprotonation of $\{\text{Me}_2\text{C}(\text{CH}=\text{NCH}_2\text{py})\}\text{M}$ ($\text{M} = \text{Cr}, \text{Co}, \text{Ni}$) creates transient azaallyls, which couple to afford three new C–C bonds about a metal–metal bond (**C**).⁵

The carbon–carbon bond formation in each case stems from a fully occupied, nonbonding orbital on the azaallyl that can be construed as having singlet diradical or ionic character.³ The former description can straightforwardly be used to rationalize

Received: April 5, 2014

Published: July 10, 2014



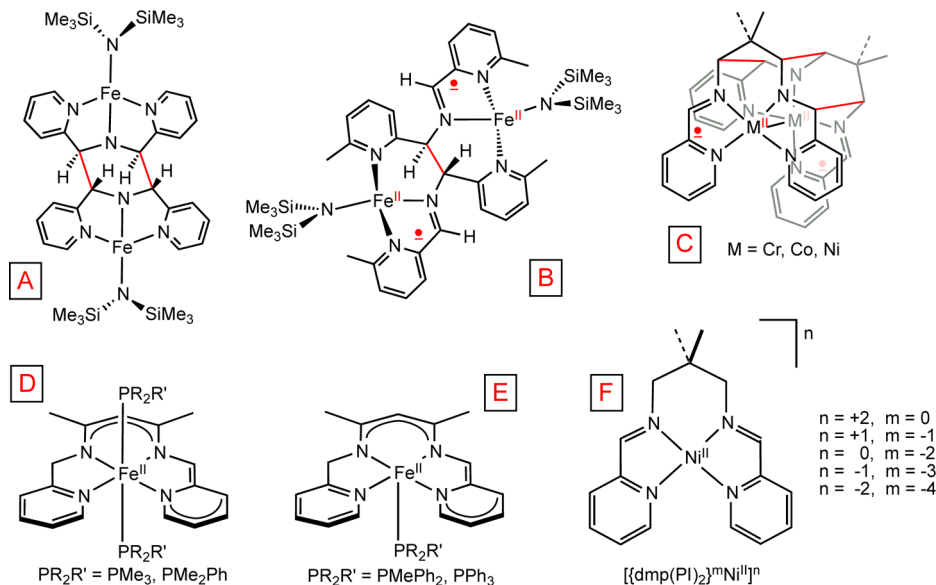


Figure 1. Whereas $[(\text{smif})\text{FeN}(\text{TMS})_2]_2$ (**A**), $[(\text{o}-\text{Me}_2-\text{smif})\text{FeN}(\text{TMS})_2]_2$ (**B**), and $\{[\text{Me}_2\text{C}(\text{CHN}=\text{CHpy})_2]\text{M}\}_2$ (**C**, $\text{M} = \text{Cr}, \text{Co}, \text{Ni}$) exhibit C–C bonds (red) derived from azaallyls, other azaallyl precursors containing nacnac ligands, namely, $\{\text{nacnac}(\text{CH}_2\text{py})(\text{CHpy})\}\text{Fe}(\text{PR}_2\text{R}')_2$ (**D**, $\text{PR}_2\text{R}' = \text{PMe}_3, \text{PMe}_2\text{Ph}$) and $\{\text{nacnac}(\text{CH}_2\text{py})(\text{CHpy})\}\text{FePR}_2\text{R}'$ (**E**, $\text{PR}_2\text{R}' = \text{PMePh}_2, \text{PPh}_3$), and pyridine-imines $\{[\text{Me}_2\text{C}(\text{CH}_2\text{N}=\text{CHpy})_2]\text{Ni}\}^n$ (**F**, $n = +2, +1, 0, -1, -2$) failed to elicit bond-making chemistry.

radical coupling processes (i.e., $\uparrow\text{CNC}\downarrow$), whereas the latter invokes the possibility of nucleophile/electrophile reactivity (i.e., ${}^+\text{C}-\text{N}-\text{C}^-$) as an alternative.

Different approaches to azaallyl precursor ligands led to unexpected results. The tetradentate chelate $\text{Me}_2\text{C}(\text{CH}_2\text{N}=\text{CHpy})_2$ was treated with $\text{Ni}(\text{COD})_2$ in anticipation of C–H bond activation leading to azaallyl species, but the pseudosquare planar neutral compound $\{\text{Me}_2\text{C}(\text{CH}_2\text{N}=\text{CHpy})_2\}\text{Ni}$ formed instead, and calculations suggested that the species contained Ni(II) and two pyridine-imine (PI) radical anions. Attempts to trigger C–C bond formation via reductive and oxidative procedures led to a remarkable series of complexes, $\{[\text{Me}_2\text{C}(\text{CH}_2\text{N}=\text{CHpy})_2]\text{Ni}\}^n$ (**F**, $n = +2, +1, 0, -1, -2$), in which the Ni(II) oxidation state may be construed as being retained, as all redox activity occurs at the ligand.⁷ The failure to observe carbon–carbon bond formation from intermediates with ligand radical character revealed the likely delocalization and persistent stability of these particular spins.

When precursors to the azaallyl functionality were incorporated into a nacnac^{8–44} framework, the expectation that related carbon–carbon bonds would form was not realized. Pseudo 20 e[−] complexes $\{\text{nacnac}(\text{CH}_2\text{py})(\text{CHpy})\}\text{Fe}(\text{PR}_2\text{R}')_2$ (**D**, $\text{PR}_2\text{R}' = \text{PMe}_3, \text{PMe}_2\text{Ph}$) were prepared,⁶ and the redox noninnocent ligand was classified as a dianion, that is, 18 e[−] $\{\text{nacnac}(\text{CH}_2\text{py})(\text{CHpy})^{2-}\}\text{Fe}^{\text{II}}(\text{PR}_2\text{R}')_2$. Removal of one phosphine to afford the monophosphine derivatives $\{\text{nacnac}(\text{CH}_2\text{py})(\text{CHpy})\}\text{FePR}_2\text{R}'$ (**E**, $\text{PR}_2\text{R}' = \text{PMePh}_2, \text{PPh}_3$) failed to elicit C–C bond formation, and calculations of the two different phosphine complexes indicated little radical character. The redox noninnocence^{45–52} of the $\{\text{nacnac}(\text{CH}_2\text{py})(\text{CHpy})\}^n$ ($n = 0, -2$) ligand did not support oxidative processes at iron, despite the promise of being a functional 2 e[−] reservoir,⁶ as in related C–C bond forming processes studied by Floriani.⁵²

In consideration of the system, it was determined that the electronic saturation at the metal was hampering the reactivity of the species; thus, a coordinatively and electronically unsaturated variant was sought. Described herein is the

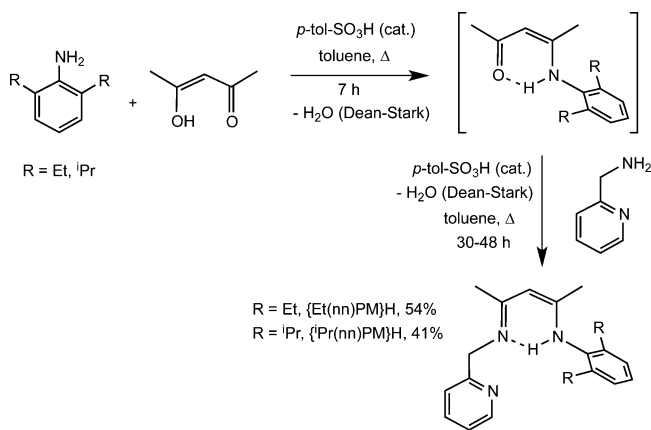
application of a nacnac framework with only one imino- or methyl-pyridine side arm, a ligand that is tridentate yet capable of being redox noninnocent in its nacnac imino-pyridine state.^{53–63} Iron and chromium were the most common metals used in this initial survey: iron because of the relation to the prior $\{\text{nacnac}(\text{CH}_2\text{py})(\text{CHpy})\}^n$ work,⁶ and chromium due to its potentially similar ground state for M(II), that is, $S = 2$, yet vastly different redox properties.

2. RESULTS

2.1. Ligand Synthesis.

Scheme 1 reveals the synthesis of the two nacnac-based tridentate ligands employed in the study.

Scheme 1



The diisopropylaniline derivative, described as $\{i\text{Pr}(\text{nn})\text{PM}\}\text{H}$, was prepared according to a literature procedure⁶⁴ in 41% yield upon crystallization from hot hexanes, and the diethyl derivative $\{\text{Et}(\text{nn})\text{PM}\}\text{H}$ was vacuum-distilled as a viscous orange oil (54%). In both instances the initial condensation occurred with acetylacetone and amine, followed by a second condensation with 2-aminomethylpyridine. Reversal of the

Scheme 2

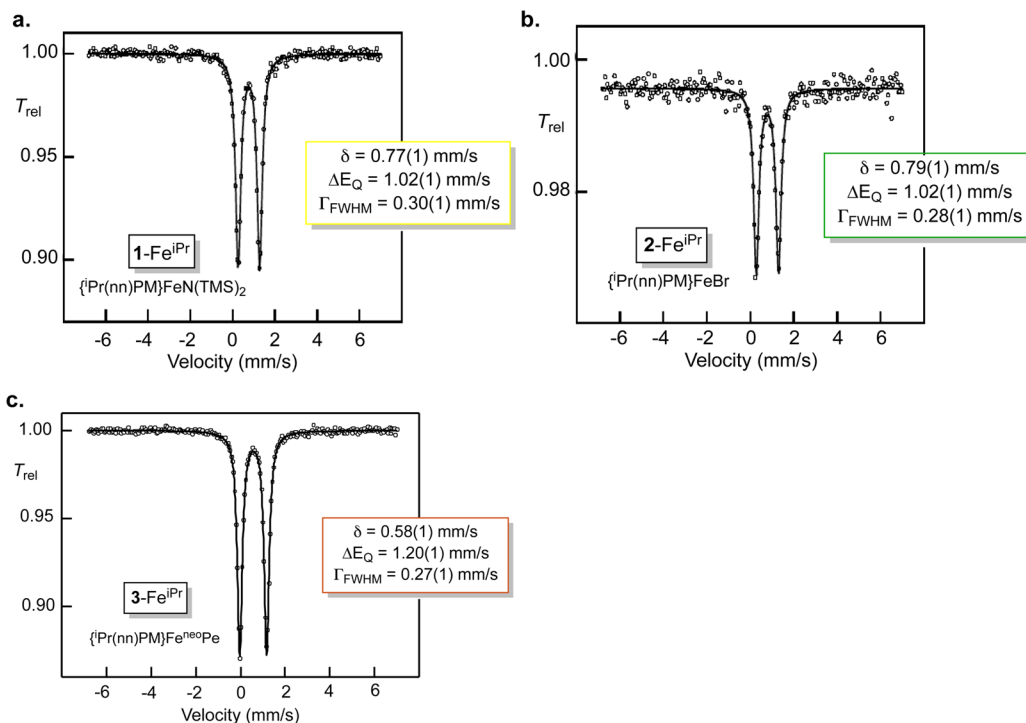
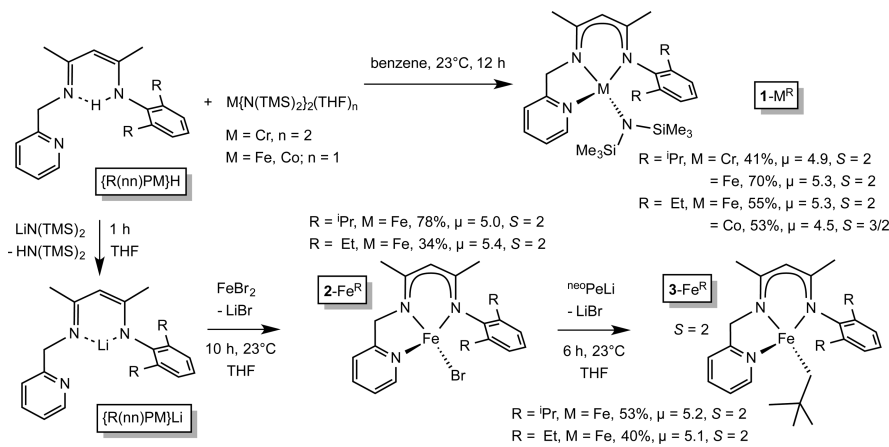


Figure 2. Zero-field Mössbauer spectra (80 K). (a.) $\{{}^{\text{i}}\text{Pr}(\text{nn})\text{PM}\}\text{FeN}(\text{TMS})_2$ ($1-\text{Fe}^{\text{iPr}}$). (b.) $\{{}^{\text{i}}\text{Pr}(\text{nn})\text{PM}\}\text{FeBr}$ ($2-\text{Fe}^{\text{iPr}}$). (c.) $\{{}^{\text{i}}\text{Pr}(\text{nn})\text{PM}\}\text{Fe}^{\text{neo}}\text{Pe}$ ($3-\text{Fe}^{\text{iPr}}$).

order invariably led to incorporation of two 2-aminomethylpyridines. The known diisopropyl ligand⁶⁴ generally afforded good solubility and excellent crystallinity, but in instances where steric effects were a concern, the diethyl derivative was an important alternative.

2.2. $\{\text{R}(\text{nn})\text{PM}\}\text{MX}$ Compounds. 2.2.1. Syntheses. Treatment of $\{{}^{\text{i}}\text{Pr}(\text{nn})\text{PM}\}\text{H}$ with metal amides $\text{M}\{\text{N}(\text{TMS})_2\}_2\text{THF}_n$ ($\text{M} = \text{Cr}$,⁶⁵ $n = 2$; $\text{M} = \text{Fe}$,⁶⁶ $\text{THF} = \text{tetrahydrofuran}$)⁶⁷ afforded the four-coordinate $\{{}^{\text{i}}\text{Pr}(\text{nn})\text{PM}\}\text{MN}(\text{TMS})_2$ ($1-\text{M}^{\text{Pr}}$; $\text{M} = \text{Cr, Fe}$) derivatives as maroon and yellow crystalline compounds in good to modest yields as Scheme 2 attests. Et derivatives $\{{}^{\text{Et}}\text{Pr}(\text{nn})\text{PM}\}\text{MN}(\text{TMS})_2$ ($1-\text{M}^{\text{Et}}$; $\text{M} = \text{Fe, Co}$) were obtained as yellow and green crystalline solids in 55% and 53% yield, respectively. Evans' method measurements⁶⁸ were conducted on samples of the amides, and the values were consistent with those of high-spin complexes. $1-\text{Cr}^{\text{iPr}}$ was found to have the spin-only value of $4.9 \mu_B$, while the two iron

compounds had slightly higher values ($\mu_{\text{eff}} = 5.3 \mu_B$), presumably due to spin-orbit coupling contributions.^{69,70}

Iron was chosen for further exploration, and the analogous green bromide complexes $\{\text{R}(\text{nn})\text{PM}\}\text{FeBr}$ ($\text{R} = \text{iPr, Et}; 2-\text{Fe}^{\text{R}}$) were prepared from ferrous bromide and $\{\text{R}(\text{nn})\text{PM}\}\text{Li}$, which was generated from the free ketamine and $\text{LiN}(\text{TMS})_2$. Bromides $2-\text{Fe}^{\text{R}}$ were alkylated with neopentylolithium to provide orange $\{\text{R}(\text{nn})\text{PM}\}\text{Fe}^{\text{neo}}\text{Pe}$ ($\text{R} = \text{iPr, Et}; 3-\text{Fe}^{\text{R}}$) in 53% and 40% yield, and both species were high-spin according to Evans' method measurements ($3-\text{Fe}^{\text{iPr}}, \mu_{\text{eff}} = 5.2$; $3-\text{Fe}^{\text{Et}}, \mu_{\text{eff}} = 5.1$), with magnetic moments slightly above the spin-only value, as is typical for iron.^{69,70}

2.2.2. Mössbauer Spectra of $\{{}^{\text{i}}\text{Pr}(\text{nn})\text{PM}\}\text{FeX}$ ($X = \text{N}(\text{TMS})_2, 1-\text{Fe}^{\text{iPr}}; \text{Br}, 2-\text{Fe}^{\text{iPr}}; \text{neoPe}, 3-\text{Fe}^{\text{iPr}}$). Zero-field Mössbauer studies^{71–73} were conducted on $\{{}^{\text{i}}\text{Pr}(\text{nn})\text{PM}\}\text{FeX}$ ($X = \text{N}(\text{TMS})_2, 1-\text{Fe}^{\text{iPr}}; \text{Br}, 2-\text{Fe}^{\text{iPr}}; \text{neoPe}, 3-\text{Fe}^{\text{iPr}}$) at 80 K, and the spectra are shown in Figure 2. The amide and bromide

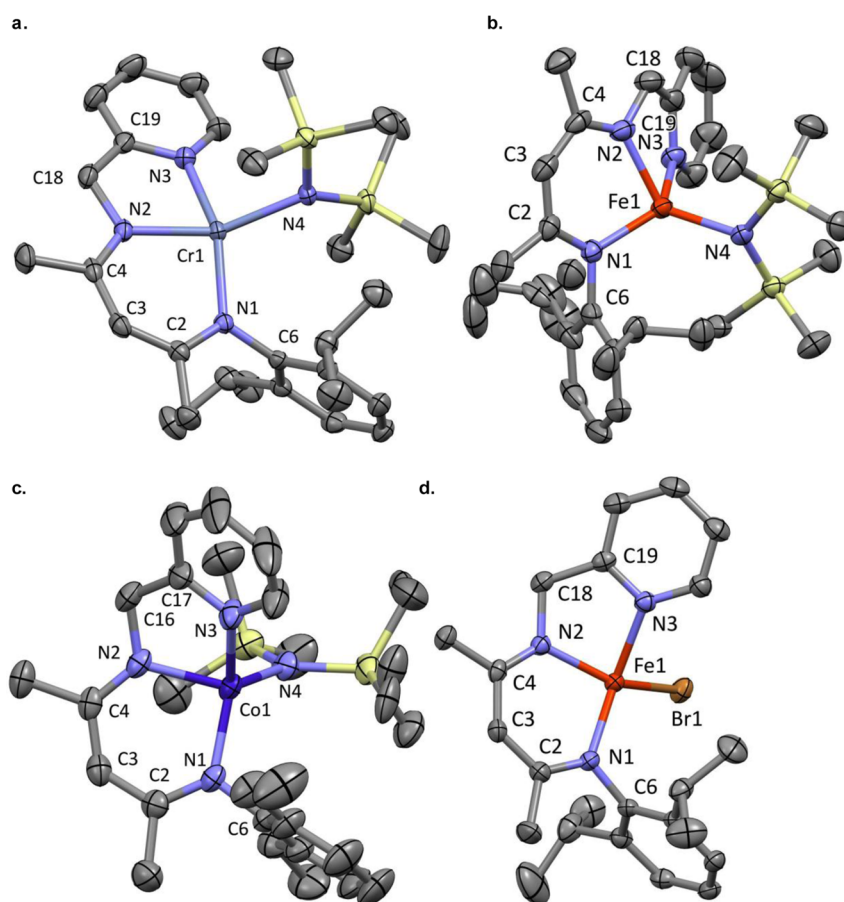
Table 1. Select Crystallographic and Refinement Data^a

9-Fe ^{Pr}									
formula	C ₂₉ H ₄₈ N ₄ S ₂ Cr	1-Cr ^{Pr}	1-Fe ^{Pr}	2-Fe ^{Pr}	4-Fe ^{Pr}	5-Fe ^{Pr}	6-Cr ₂ Fe ^{Pr}	7-Fe ^{Pr}	8-Fe _{Et}
form wt	560.89	C ₂₉ H ₄₈ N ₄ S ₂ Fe	C ₂₇ H ₄₄ N ₄ S ₂ Co	C ₂₃ H ₄₀ N ₃ BrFe	C ₃₀ H ₄₁ N ₃ O ₂ Fe	C ₃₉ H ₄₁ N ₃ O ₄ Cr	C ₅₃ H ₆₀ N ₃ Cl ₂ Fe ₂	C ₄₂ H ₅₀ N ₆ Fe	C ₇₂ H ₈ N ₈ Fe ₂
space gp	P $\overline{1}$	564.74	539.77	484.26	531.51	459.36	95.69	694.73	1167.12
Z	2	P $\overline{1}$	P $\overline{1}/c$	P $\overline{1}/c$	P $\overline{1}$	P $\overline{1}$	P $\overline{1}/c$	P $\overline{1}2_1$	P $\overline{1}ca$
a, Å	11.0716(8)	8.7885(6)	11.9196(4)	12.2363(6)	9.1288(7)	8.9026(5)	9.6836(7)	19.624(2)	18.765(4)
b, Å	11.5269(8)	11.7993(8)	16.2443(5)	11.8702(6)	10.9934(8)	9.0038(6)	13.1687(9)	11.6591(14)	15.7753(3)
c, Å	15.1284(11)	15.8360(10)	15.5843(5)	15.9743(8)	15.2486(12)	15.4509(10)	14.8173(10)	16.056(6)	16.0964(17)
α , deg	91.882(4)	98.584(4)	90	90	85.922(3)	90.636(2)	97.047(2)	90	90
β , deg	109.554(3)	96.246(4)	94.9870(10)	101.9250(10)	88.695(3)	103.810(2)	102.152(3)	102.446(8)	90
γ , deg	117.600(3)	100.285(4)	90	90	69.620(3)	110.307(2)	107.505(2)	90	90
V, Å ³	1570.97(19)	1583.96(18)	3006.10(17)	2270.0(2)	1430.99(19)	1129.41(12)	1726.2(2)	5494(3)	3692.4(7)
$\rho_{\text{calc}}^{\text{exp}}$ g·cm ⁻³	1.186	1.184+	1.193	1.417	1.234	1.351	1.285	1.155	1.250
μ , mm ⁻¹	0.575	0.671	2.437	0.557	0.694	0.376	0.662	0.447	0.510
temp, K	173(2)	193(2)	183(2)	173(2)	173(2)	173(2)	173(2)	173(2)	183(2)
λ , Å	0.71073	0.71073	0.71073	0.71073	0.71073	0.71073	0.71073	0.71073	0.71073
R indices	R ₁ = 0.0456	R ₁ = 0.0378	R ₁ = 0.0280	R ₁ = 0.0348	R ₁ = 0.0272	R ₁ = 0.0320	R ₁ = 0.0391	R ₁ = 0.0463	R ₁ = 0.0420
[I > 2σ(I)] ^{b,c}	wR ₂ = 0.0839	wR ₂ = 0.0842	wR ₂ = 0.0727	wR ₂ = 0.0754	wR ₂ = 0.0868	wR ₂ = 0.0896	wR ₂ = 0.0722	wR ₂ = 0.1020	wR ₂ = 0.1020
R indices ^c	R ₁ = 0.0597	R ₁ = 0.0609	R ₁ = 0.0382	R ₁ = 0.0469	R ₁ = 0.0310	R ₁ = 0.0368	R ₁ = 0.0618	R ₁ = 0.0914	R ₁ = 0.0744
(all data) ^b	wR ₂ = 0.0931	wR ₂ = 0.0947	wR ₂ = 0.0970	wR ₂ = 0.0984	wR ₂ = 0.0785	wR ₂ = 0.0907	wR ₂ = 0.0969	wR ₂ = 0.0862	wR ₂ = 0.1176
GOF ^d	1.027	1.034	1.011	1.037	1.064	1.020	1.030	1.002	0.996

^aData relate to compounds {R(nn)PM}{MN(TMS)₂} (R = ¹Pr, M = Cr, ¹Cr^{Pr}, Fe, ¹Fe^{Pr}, R = Et, M = Co, ¹Co^{Pr}, ²FeBr (2-Fe^{Pr}), {¹Pr(nn)PM}{FeBr (2-Fe^{Pr})}, {¹Pr(nn)PM}{Fe(CO^{neop})CO (4-Fe^{Pr})}, {¹Pr(nn)P(OC₂H₅)₂Cr(CO)₂ (5-Cr^{Pr}), {¹Pr(nn)CHPy₂FeCl₂ (7-Fe^{Pr}), {¹Pr(nn)CHPy₂Fe (8-Fe^{Pr}), and {¹Pr(nn)CHPy₂(FeN=CPh₂)₂ (9-Fe^{Pr}). *b*, $R_I = \Sigma |F_0| - |F_{\parallel}| / \Sigma |F_0|$ – number of independent reflections; *p* = number of parameters.

Table 2. Selected Interatomic Distances (\AA) and Angles (deg)^a

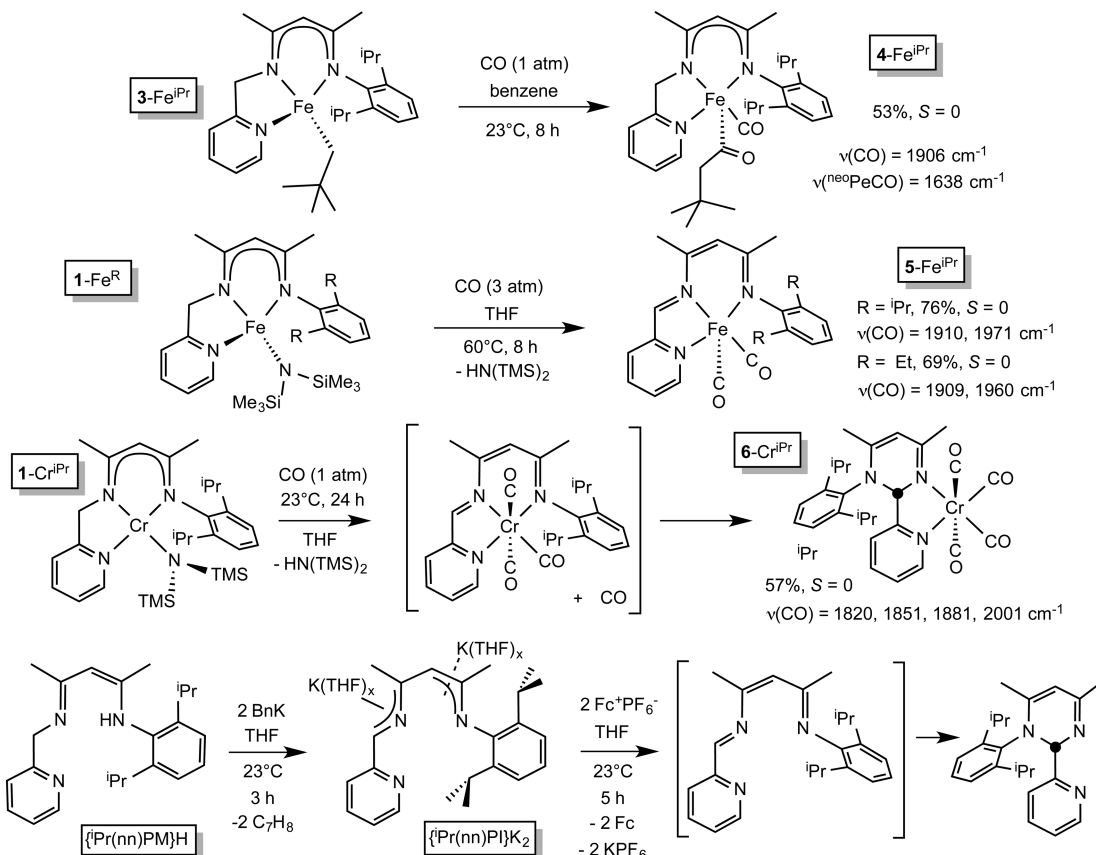
	1-Cr ^{iPr}	1-Fe ^{iPr}	1-Co ^{Et} ^b	2-Fe ^{iPr}
M–N1	2.076(2)	2.029(2)	1.974(2)	2.007(2)
M–N2	2.045(2)	2.036(2)	1.978(2)	2.030(2)
M–N3	2.120(2)	2.201(2)	2.108(2)	2.127(2)
M–N4/Br	2.071(2)	1.967(2)	1.955(2)	2.4146(3)
N1–C6	1.447(2)	1.446(3)	1.435(3)	1.446(2)
N1–C2	1.337(2)	1.333(3)	1.334(3)	1.335(2)
C2–C3	1.399(3)	1.407(4)	1.401(4)	1.403(2)
C3–C4	1.393(3)	1.393(4)	1.401(4)	1.404(3)
C4–N2	1.331(2)	1.313(4)	1.324(3)	1.320(2)
N2–C18/C16	1.464(2)	1.458(4)	1.452(3) ^b	1.459(2)
C18/C16–C19/C17	1.493(3)	1.495(5)	1.495(4) ^b	1.511(3)
C19/C17–N3	1.343(2)	1.344(3)	1.354(3) ^b	1.341(2)
N4–Si(ave)	1.706(7)	1.708(14)	1.708(2)	
N1–M–N2	90.07(6)	90.08(9)	93.41(9)	92.19(6)
N1–M–N3	156.06(6)	131.56(8)	125.83(9)	141.39(6)
N1–M–N4/Br	106.15(6)	121.89(8)	117.18(9)	111.22(4)
N2–M–N3	78.49(6)	76.87(9)	79.20(9)	78.02(6)
N2–M–N4/Br	152.25(6)	130.84(9)	122.85(9)	145.73(4)
N3–M–N4/Br	93.06(6)	100.56(8)	111.30(9)	96.16(4)

^aData relate to compounds $\{\text{R(nn)}\text{PM}\}\text{MN}(\text{TMS})_2$ ($\text{R} = \text{iPr}$, $\text{M} = \text{Cr}$, **1-Cr**^{iPr}; Fe , **1-Fe**^{iPr}; $\text{R} = \text{Et}$, $\text{M} = \text{Co}$, **1-Co**^{Et}), and $\{\text{iPr(nn)}\text{PM}\}\text{FeBr}$ (**2-Fe**^{iPr}).^bFor **1-Co**^{Et}, the corresponding distances are N2–C16, C16–C17, N3–C17.Figure 3. Molecular views of $\{\text{R(nn)}\text{PM}\}\text{MN}(\text{TMS})_2$ ($\text{R} = \text{iPr}$, $\text{M} = \text{Cr}$, **1-Cr**^{iPr} (a.); Fe , **1-Fe**^{iPr} (b.); $\text{R} = \text{Et}$, $\text{M} = \text{Co}$, **1-Co**^{Et} (c.)), and $\{\text{iPr(nn)}\text{PM}\}\text{FeBr}$ (**2-Fe**^{iPr} (d.)).

derivatives have essentially identical spectra, with isomer shifts of 0.77 and 0.79 mm/s, respectively, and quadrupole splittings of 1.02 mm/s. The values are consistent with high-spin ferrous samples in a modestly asymmetric environment and point

toward pseudotetrahedral rather than pseudosquare planar coordination. The similarity in spectra strongly suggests that the field strengths of $(\text{TMS})_2\text{N}^-$ and Br^- are remarkably similar but significantly different than the neopentyl derivative, whose

Scheme 3



$\delta = 0.58$ mm/s and $\Delta E_Q = 1.20$ mm/s represent a higher field strength and an environment relatively more toward square planar, yet still within the high-spin Fe(II) range.

2.2.2. Structural Studies of $\{R(nn)PM\}MX$ ($R = ^iPr$, $X = N(TMS)_2$, $M = Cr, Fe, 1-M^{iPr}$; $R = Et$, $X = N(TMS)_2$, $M = Co, 1-Co^{Et}$; $R = ^iPr$, $X = Br$, $M = Fe, 2-Fe^{iPr}$). Table 1 provides selected crystallographic and refinement details for $\{R(nn)PM\}MNT(TMS)_2$ ($R = ^iPr, M = Cr, 1-Cr^{iPr}$; $Fe, 1-Fe^{iPr}$; $R = Et, M = Co, 1-Co^{Et}$) and $\{Pr(nn)PM\}FeBr$ ($2-Fe^{iPr}$), and Table 2 lists pertinent metric parameters, while Figure 3 provides molecular views of the molecules. All the complexes are considerably distorted from either T_d or square planar geometries, with the constraints of the chelate responsible for supplying most of the deviations.

For each species, the distances around the ligand are quite similar, and the charge distribution in the nacnac portion of the chelate appears to be even, as $d(C_2-C_3)$ and $d(C_3-C_4)$ range from 1.39 to 1.41 Å, and $d(N_1-C_2)$ and $d(N_2-C_4)$ range from 1.31 to 1.34. The longest $d(M-N)$ is from the metal to the pyridine nitrogen, the likely weakest donor, and the metal–nitrogen distances within the nacnac are significantly shorter by 0.05–0.12 Å. The bond lengths correspond to periodic tendencies as the Cr(II) distances are longer than the Fe(II) species, with the cobalt(II) complex having the shortest.

The most interesting metrics concern the core bond angles. The nacnac bite angle is slightly smaller for $1-Cr^{iPr}$ and $1-Fe^{iPr}$ at $\sim 90.1^\circ$ compared to $93.41(9)^\circ$ and $92.19(6)^\circ$ for $1-Co^{Et}$ and $2-Fe^{iPr}$, respectively. Likewise, the $N_{py}-M-N_{nn}$ angles average $78.1(10)^\circ$, and the differences in either set are too small to merit discussion. The opposing $N_{py}-M-N_{nn}$ angles are quite different, and deserve consideration, with that of $1-Cr^{iPr}$

($156.06(6)^\circ$) $>$ $2-Fe^{iPr}$ ($141.39(6)^\circ$) $>$ $1-Fe^{iPr}$ ($131.56(8)^\circ$) $>$ $1-Co^{Et}$ ($125.83(9)^\circ$). This angle correlates with the N_2-M-N_4/Br angle, and together they indicate the deviation from square planar geometry in this system: $1-Cr^{iPr}$ ($152.25(6)^\circ$) $<$ $2-Fe^{iPr}$ ($145.73(4)^\circ$) $<$ $1-Fe^{iPr}$ ($130.84(9)^\circ$) $<$ $1-Co^{Et}$ ($122.85(9)^\circ$). The cobalt species manifests the greatest distortion away from square planar; both ferrous derivatives are next and are relatively similar, substantiating the claim based on the Mössbauer spectra regarding like field strengths, and the chromium complex is the closest to pseudosquare planar. The remaining angles complement these observations.

2.3. Carbonylations of $\{R(nn)PM\}MX$ ($R = ^iPr$, $X = N(TMS)_2$, $M = Cr, Fe, 1-M^{iPr}$; $X = ^{neop}Pe$, $M = Fe, 3-Fe^{iPr}$).

2.3.1. Carbonylations. Initial reactivity studies were conducted on $\{^iPr(nn)PM\}Fe^{neop}Pe$ ($3-Fe^{iPr}$), but the complex failed to eliminate ^{neop}PeH under various conditions, including hydrogenation. No olefin reactivity was found, and no sign of olefin hydrogenation activity was detected. Next, $3-Fe^{iPr}$ was treated with CO, and a relatively swift conversion to the acyl carbonyl $\{^iPr(nn)PM\}Fe(CO)^{neop}PeCO$ ($4-Fe^{iPr}$) occurred over an 8 h period at $23^\circ C$ (Scheme 3). The infrared spectrum of $4-Fe^{iPr}$ showed two carbonyl stretching frequencies, one at 1906 cm^{-1} corresponding to the terminal carbonyl, and one at 1638 cm^{-1} pertaining to the acyl. Attempts to convert the acyl into a Fischer-type carbene failed, and hydrogenation attempts to release aldehyde were also unsuccessful.

Previous work on $\{PM(nn)PM\}FeN(TMS)_2$ revealed that the addition of ligands could induce $HN(TMS)_2$ loss,⁶ thus $\{R(nn)PM\}FeN(TMS)_2$ ($R = ^iPr, 1-Fe^{iPr}; Et, 1-Fe^{Et}$) was exposed to 1 atm CO for 8 h at $60^\circ C$ to afford $\{R(nn)PI\}Fe(CO)_2$ ($R = ^iPr, 5-Fe^{iPr}; Et, 5-Fe^{Et}$) in good

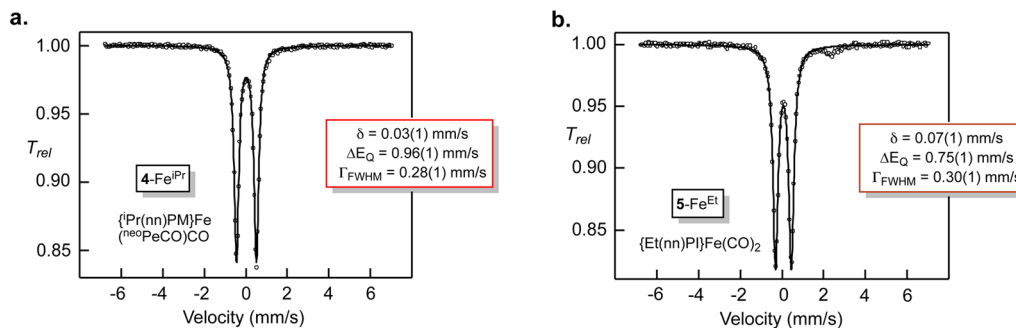


Figure 4. Zero-field Mössbauer spectra (80 K) of (a.) $\{\text{Pr}(\text{nn})\text{PM}\}\text{Fe}(\text{CO}^{\text{neo}}\text{Pe})\text{CO}$ (**4-Fe^{iPr}**) and (b.) $\{\text{Et}(\text{nn})\text{PI}\}\text{Fe}(\text{CO})_2$ (**5-Fe^{Et}**).

yields, as shown in Scheme 3. The dark blue diamagnetic complexes each possessed two terminal CO stretches in their IR spectra (**5-Fe^{iPr}**, 1910, 1971 cm⁻¹; **5-Fe^{Et}**, 1909, 1960 cm⁻¹), and ¹H NMR signals consistent with an unsaturated nacnac-imino-pyridine backbone formed from loss of HN(TMS)₂. Expectations were that the corresponding chromium compound $\{\text{Pr}(\text{nn})\text{PM}\}\text{CrN}(\text{TMS})_2$ (**1-Cr^{iPr}**) would undergo the same HN(TMS)₂ loss to provide a tricarbonyl complex. Loss of amine was noted after 24 h at 23 °C under 1 atm CO, but IR spectra of the yellow-orange diamagnetic product revealed four terminal CO bands at 1820, 1851, 1881, and 2001 cm⁻¹ whose intensities did not vary upon recrystallization. The position of the “imine” proton in the ¹H NMR spectrum at δ 5.36 was conspicuously distinct from that of **5-Fe^{iPr}** (δ 7.81) and **5-Fe^{Et}** (δ 7.83), rendering the unsaturated ligand backbone questionable. An X-ray crystallographic structure determination identified the ligand as a bidentate nitrogen donor, namely, 2-H,2-pyridyl-3-DIPP-4,6-dimethylpyrimidine, hence the compound is $\{\kappa^2-\text{N},\text{N}-2-\text{H},2-\text{pyridyl}-3-\text{DIPP}-4,6-\text{dimethylpyrimidine}\}\text{Cr}(\text{CO})_4$, abbreviated as $\{\kappa^2-\text{N},\text{N}-\text{pyrim-pyr}\}\text{Cr}(\text{CO})_4$ (**6-Cr^{iPr}**).

Scheme 3 shows a plausible path for the formation of $\{\kappa^2-\text{N},\text{N}-\text{pyrim-pyr}\}\text{Cr}(\text{CO})_4$ (**6-Cr^{iPr}**) via the CO-induced loss of HN(TMS)₂ from **1-Cr^{iPr}** to afford an intermediate $\{\text{Pr}(\text{nn})\text{PI}\}\text{Cr}(\text{CO})_3$ species, which can undergo N_{nn} migration to the pyridine-imine. The $\{\text{Pr}(\text{nn})\text{PI}\}$ ligand is directly related to the previously studied $\{\text{nacnac}(\text{CH}_2\text{py})(\text{CHpy})\}^n$ ($n = 0, -1, -2$) tetradentate chelate,⁶ and it is plausible that it can function as a 12 πe^- neutral, 13 e^- monoanionic, or 14 e^- dianionic species, but not all may be stable in regard to their respective Cr(0), Cr(I), or Cr(II) environment. To test the susceptibility of $\{\text{Pr}(\text{nn})\text{PI}\}^n$ ($n = 0, -1, -2$) to cyclization, the dianion was generated from $\{\text{Pr}(\text{nn})\text{PM}\}\text{H}$ via double deprotonation by potassium benzyl. The dianion was found to be stable, but when subjected to oxidation by ferricinium (i.e., $(\text{Cp}_2\text{Fe})^+\text{PF}_6^-$), cyclization occurred rapidly, indicating the monoanion, the neutral, or both were unstable with respect to pyrimidine formation. It is unlikely that $\{\text{Pr}(\text{nn})\text{PI}\}^{2-}$ is stable as a ligand for $\text{Cr}(\text{CO})_n^{2+}$, where carbonyl ligation aids in effectively increasing the oxidizing capability of the chromium.

2.3.2. Mössbauer Spectra of $\{\text{Pr}(\text{nn})\text{PM}\}\text{Fe}(\text{CO}^{\text{neo}}\text{Pe})\text{CO}$ (4-Fe^{iPr}**) and $\{\text{R}(\text{nn})\text{PI}\}\text{Fe}(\text{CO})_2$ ($\text{R} = \text{iPr}$, **5-Fe^{iPr}**; Et , **5-Fe^{Et}**).** From the standpoint of formal oxidation state, the acyl carbonyl complex $\{\text{Pr}(\text{nn})\text{PM}\}\text{Fe}(\text{CO}^{\text{neo}}\text{Pe})\text{CO}$ (**4-Fe^{iPr}**) is clearly Fe(II); the nacnac and acyl are both closed-shell anions in a conventional sense. The Mössbauer spectrum of **4-Fe^{iPr}** reveals an isomer shift of δ 0.03(1) mm/s, which is an atypical region for most ferrous species, but in a region similar to that found for $\text{Fe}(\text{CO})_5$ and $\text{Fe}(\text{CO})_4\text{PPh}_3$ ($\sim\delta 0.10$ mm/s)^{74–77} (Figure

4). Its modest ΔE_Q of 0.96(1) mm/s is in line with the asymmetry found in pseudo square pyramidal complexes. The isomer shift is below that found (δ 0.14 mm/s) for $\{\text{nn}(\text{PM})(\text{PI})\}\text{FeCO}$, which has been shown computationally and via structural metrics to be best considered Fe(II).⁶ It appears that the two highly covalent ligands, namely, CO and ^{neo}PeCO, are enough to render the isomer shift quite low relative to typical octahedral ferrous complexes.⁷⁸

In line with the acyl complex, the Mössbauer spectrum of $\{\text{Et}(\text{nn})\text{PI}\}\text{Fe}(\text{CO})_2$ (**5-Fe^{Et}**) is consistent with a high degree of covalency. The isomer shift of 0.07(1) mm/s for **5-Fe^{Et}** is quite low, but in a region that can correspond to Fe(0) or Fe(II) complexes, depending on the degree of covalency in the bonding, and again the carbonyl ligands are found to be very effective at promoting covalency^{79,80} (Figure 4). The ΔE_Q value of 0.75(1) mm/s for **5-Fe^{Et}** is fairly low for a five-coordinate complex and suggests that a relatively symmetric electronic environment exists for the dicarbonyl.

2.3.3. Structural Studies of $\{\text{Pr}(\text{nn})\text{PM}\}\text{Fe}(\text{CO}^{\text{neo}}\text{Pe})\text{CO}$ (4-Fe^{iPr}**), $\{\text{Pr}(\text{nn})\text{PI}\}\text{Fe}(\text{CO})_2$ (**5-Fe^{iPr}**), and $\{\kappa^2-\text{N},\text{N}-\text{pyrim-pyr}\}\text{Cr}(\text{CO})_4$ (**6-Cr^{iPr}**).** Selected data acquisition and refinement details for the carbonylation products are listed in Table 1, while metric parameters may be found in the captions of the figures featuring their respective molecular views. In Figure 5, $\{\text{Pr}(\text{nn})\text{PM}\}\text{Fe}(\text{CO}^{\text{neo}}\text{Pe})\text{CO}$ (**4-Fe^{iPr}**) is found to be a square pyramid with an apical ^{neo}PeCO ligand and basal nacnac(PM) and carbonyl ligands. With the exception of the N_{py}–Fe–N_{nn} angle of 82.05(5)°, which is essentially mandated by the chelate bite (see Table 2), the core angles vary between 90.79(6)° (C_{acyl}–Fe–C_{CO}) and 101.21(5)° (N_{nn}–Fe–C_{acyl}), thus determining the regular nature of the square pyramid. Even the trans-basal angles of 162.07(5)° (N_{nn}–Fe–N_{py}) and 173.07(5)° (N_{nn}–Fe–C_{CO}) indicate little distortion.

The bond distances of the nacnac are symmetric, and all the Fe–N distances are short relative to the previously listed bond lengths of the high-spin four-coordinate compounds (Table 2). The acyl is also short at 1.908(2) Å, and the carbonyl exhibits parameters indicative of strong π backbonding: d(Fe–C_{CO}) = 1.754(2) Å and d(C_{CO}–O) = 1.154(2) Å. All indications point toward a highly covalent molecule with relatively tight bonds to all core atoms.

Illustrated in Figure 6 is a molecular view of the iron dicarbonyl $\{\text{Pr}(\text{nn})\text{PI}\}\text{Fe}(\text{CO})_2$ (**5-Fe^{iPr}**), whose structure is also a very regular square pyramid, although with slightly more distortion than **4-Fe^{iPr}**. Note that the metric parameters defining the pyridine-imine arm of the chelate leave the redox character of the $\{\text{Pr}(\text{nn})\text{PI}\}^n$ ligand somewhat debatable. In comparison to the previously studied $\{\text{nn}(\text{PM})(\text{PI})\}^n$ tetradentate chelate,⁶ d(N3–C19) = 1.383(2) Å, d(C18–C19) =

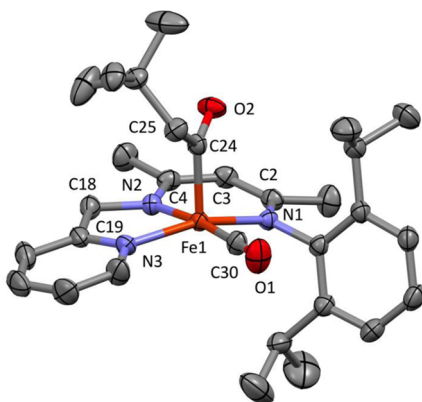


Figure 5. Molecular view of $\{^i\text{Pr}(\text{nn})\text{PM}\}\text{Fe}(\text{CO}^{\text{neo}}\text{Pe})\text{CO}$ (**4-Fe^{iPr}**). Selected interatomic distances (Å) and angles (deg): Fe–N1, 1.938(2); Fe–N2, 1.926(2); Fe–N3, 1.971(2); Fe–C24, 1.908(2); Fe–C30, 1.754(2); N1–C2, 1.332(2); C2–C3, 1.396(2); C3–C4, 1.385(2); N2–C4, 1.331(2); N2–C18, 1.459(2); C18–C19, 1.486(2); N3–C19, 1.343(2); C24–O2, 1.211(2); C30–O1, 1.154(2); C24–C25, 1.528(2); N1–Fe–N2, 92.16(5); N1–Fe–N3, 162.07(5); N1–Fe–C24, 101.21(5); N1–Fe–C30, 92.82(5); N2–Fe–N3, 82.05(5); N2–Fe–C24, 92.96(5); N2–Fe–C30, 173.07(5); N3–Fe–C24, 96.04(5); N3–Fe–C30, 91.77(6); C24–Fe–C30, 90.79(6); Fe–C24–O2, 116.8(2); Fe–C30–O1, 175.2(2).

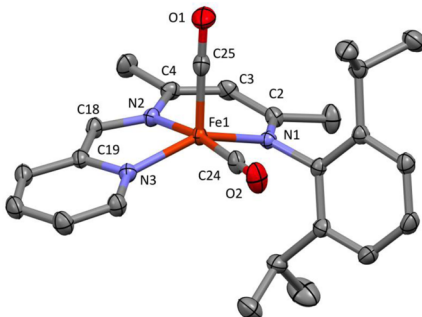


Figure 6. Molecular view of $\{^i\text{Pr}(\text{nn})\text{PI}\}\text{Fe}(\text{CO})_2$ (**5-Fe^{iPr}**). Selected interatomic distances (Å) and angles (deg): Fe–N1, 1.962(2); Fe–N2, 1.944(2); Fe–N3, 1.952(2); Fe–C24, 1.779(2); Fe–C25, 1.766(2); N1–C2, 1.321(2); C2–C3, 1.416(2); C3–C4, 1.367(2); N2–C4, 1.372(2); N2–C18, 1.355(2); C18–C19, 1.388(2); N3–C19, 1.383(2); C24–O2, 1.149(2); C25–O1, 1.151(2); N1–Fe–N2, 90.73(4); N1–Fe–N3, 146.53(4); N1–Fe–C24, 93.43(5); N1–Fe–C25, 103.48(5); N2–Fe–N3, 80.80(4); N2–Fe–C24, 171.08(5); N2–Fe–C25, 95.33(5); N3–Fe–C24, 91.43(5); N3–Fe–C25, 109.50(5); C24–Fe–C25, 91.37(6); Fe–C24–O2, 174.8(2); Fe–C25–O1, 178.7(2).

1.388(2) Å, d(N2–C18) = 1.355(2) Å, d(N2–C4) = 1.372(2) Å, d(C3–C4) = 1.367(2) Å, and d(C2–C3) = 1.416(2) Å are sufficiently ambiguous to render the redox assignment difficult. The ambiguity in assignment is not helped by either the Mössbauer studies or the IR spectra, since Fe(0)–Fe(II) oxidation states can be accommodated by both spectroscopies.

The square pyramid is only slightly distorted toward tbp by a significant cant of the opposing $\text{N}_{\text{nn}}\text{–Fe–N}_{\text{py}}$ angle of 146.53(4)°. Aside from the adjacent $\text{N}_{\text{nn}}\text{–Fe–N}_{\text{py}}$ angle of 80.80(4), the remaining core angles are between 90.73(5)° (N1–Fe–N2) and 109.50(5)° (N3–Fe–C25), and N2–Fe–C24 is 171.08(5)°. Including the d(Fe–C) of 1.779(2) and 1.766(2) Å, the bond distances of the core are very similar to those of the acyl-carbonyl **4-Fe^{iPr}**, with the chelate distances ~0.008 Å longer in total.

The chromium tetracarbonyl $\{\kappa^2\text{-N,N-pyrim-pyr}\}\text{Cr}(\text{CO})_4$ (**6-Cr^{iPr}**) is a pseudo-octahedral species with the bidentate N-donor chelate occupying cis positions (Figure 7). The CO

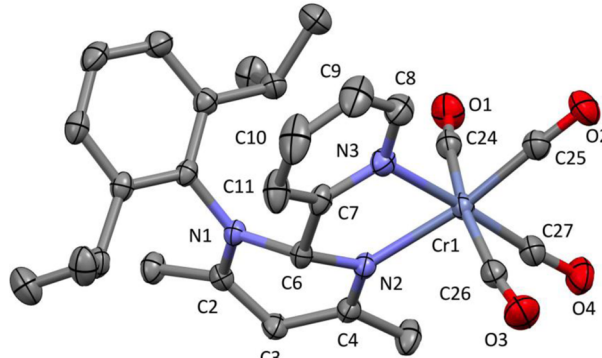


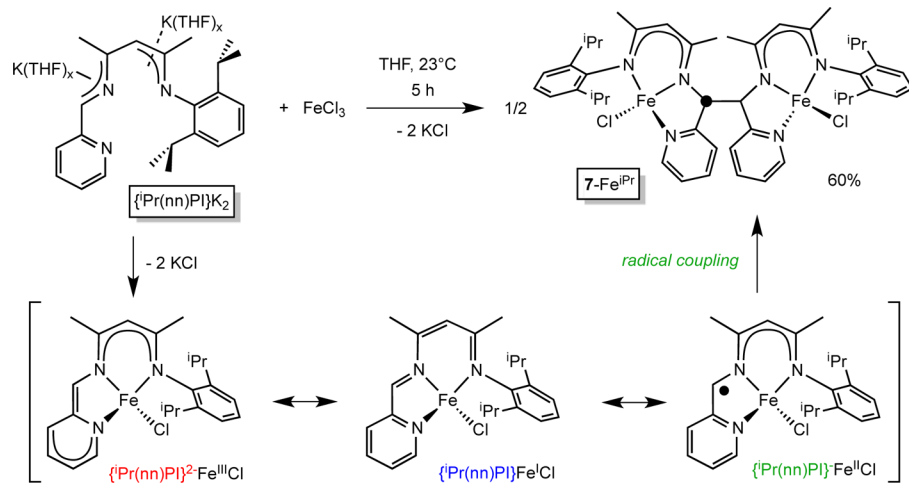
Figure 7. Molecular view of $\{\kappa^2\text{-N,N-pyrim-pyr}\}\text{Cr}(\text{CO})_4$ (**6-Cr^{iPr}**). Selected interatomic distances (Å) and angles (deg): Cr–N2, 2.139(2); Cr–N3, 2.132(2); Cr–C24, 1.895(2); Cr–C25, 1.840(2); Cr–C26, 1.910(2); Cr–C27, 1.826(2); N1–C6, 1.498(2); N1–C2, 1.353(2); C2–C3, 1.374(2); C3–C4, 1.425(2); N2–C4, 1.307(2); N2–C6, 1.463(2); C6–C7, 1.508(2); N3–C7, 1.344(2); N3–C8, 1.350(2); C24–O1, 1.149(2); C25–O2, 1.157(2); C26–O3, 1.141(2); C27–O4, 1.169(2); N2–Cr–N3, 75.91(4); N2–Cr–C24, 91.10(5); N2–Cr–C25, 169.96(5); N2–Cr–C26, 94.28(5); N2–Cr–C27, 103.62(5); N3–Cr–C24, 100.59(5); N3–Cr–C25, 94.19(5); N3–Cr–C26, 90.23(5); N3–Cr–C27, 174.97(5); C24–Cr–C25, 89.09(6); C24–Cr–C26, 168.82(6); C24–Cr–C27, 84.41(6); C25–Cr–C26, 87.31(6); C25–Cr–C27, 86.39(6); C26–Cr–C27, 84.80(6); C7–C6–N1, 112.39(9); C7–C6–N2, 110.07(9); C6–N1–C2, 113.16(9); N1–C2–C3, 118.70(10); C2–C3–C4, 117.57(11); C3–C4–N2, 121.43(9); C4–N2–C6, 111.76(10); N1–C6–N2, 111.18(9).

ligands opposite the $\kappa^2\text{-N,N-donor}$ are significantly shorter (1.840(2), 1.826(2) Å) than those mutually trans (1.895(2), 1.910(2) Å), thereby revealing the significant trans influence of the carbonyl ligand and the corresponding d(CO) correlate as expected, with longer bond lengths attributed to those opposite the N-donors. The nitrogen of the pyridine half of the chelate is bound at a slightly shorter distance (2.132(2) Å) than that of the hydro-pyrimidine (2.139(2) Å), which is clearly sp^3 -hybridized at C6, the carbon attached to the pyridine. Within the pyrimidine, the nitrogen–carbon distances are significantly different and can be construed as single ($d(\text{N1–C2}) = 1.353(2)$ Å) and double ($d(\text{N2–C4}) = 1.307(2)$ Å) bonds in conjugation,⁸¹ as are the carbon–carbon distances, which clearly show C2–C3 as a double bond (1.374(2) Å), and C3–C4 as a short, conjugated single bond (1.425(2) Å).

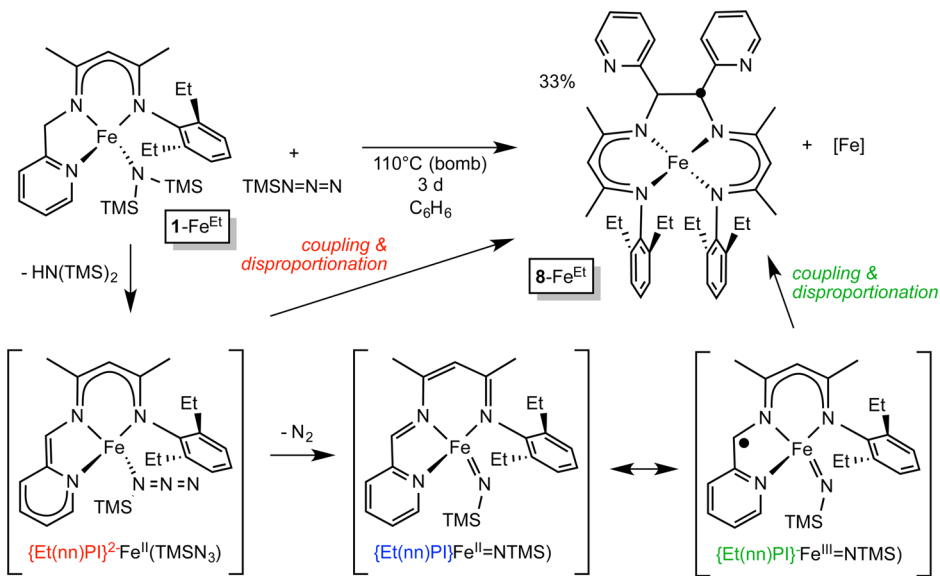
2.4. Oxidatively Induced Carbon–Carbon Bond-Forming Reactions of $\{\text{R}(\text{nn})\text{PI}\}\text{MX}/\text{L}$. **2.4.1. $\{^i\text{Pr}(\text{nn})\text{PI}\}^{2-}$ and Ferric Chloride.** The preceding carbonylation studies showed that formation of a pyridine-imine nacnac framework could be induced by addition of CO, but the resulting π system did not afford any C–C coupling, despite the potential for such events at the imine carbon and mid-nacnac carbon. Historically, FeCl_3 has been a reagent used in C–C bond formation;^{82,83} hence, generation of ferric complexes might be a means to initiate the desired reactivity.

As Scheme 4 illustrates, treatment of $[\{^i\text{Pr}(\text{nn})\text{PI}\}^{2-}] \cdot (\text{K}^+(\text{THF})_x)_2$ with FeCl_3 in THF afforded a yellow product, $\{^i\text{Pr}(\text{nn})\text{CHPy}\}_2\text{Fe}_2\text{Cl}_2$ (**7-Fe^{iPr}**, 60%), in which a new C–C bond has been formed via coupling of the imine carbons. Since

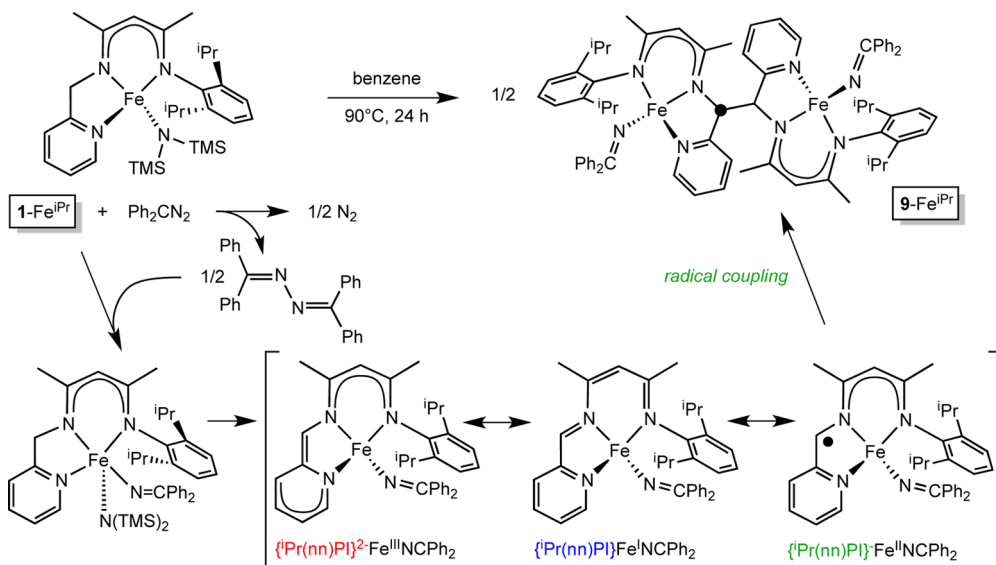
Scheme 4



Scheme 5



Scheme 6



7-Fe^{iPr} is paramagnetic and composed of two $S = 2$ centers (μ_{eff} (Evans) = $6.4 \mu_B$), the ^1H NMR spectrum of the crude reaction mixture was of limited utility in identifying potential isomers. The C_2 structure of **7-Fe^{iPr}** was obtained via X-ray crystallographic studies, and is likely to be the main component, but the related C_i structure cannot be ruled out as a minor product. Formation of complex **7-Fe^{iPr}** can be rationalized as a simple coupling of the Fe(II) form of the corresponding monomeric chloride, which can be viewed as having radical character at the imine carbon, as Scheme 4 illustrates.

2.4.2. $\{\text{Et}(nn)\text{PM}\}\text{FeN}(\text{TMS})_2$ (1-Fe^{Et}) and TMSN_3 . Exposure of $\{\text{Et}(nn)\text{PM}\}\text{FeN}(\text{TMS})_2$ (1-Fe^{Et}) to TMSN_3 had two potentially positive outcomes: the synthesis of an imido derivative or the oxidative triggering of C–C bond formation. As Scheme 5 indicates, the latter was found upon heating the reagents for 3 d at 110°C in THF, but the coupling occurred with disproportionation, yielding the green, tetradeinate chelate complex $\{\text{[Et}(nn)\text{CHpy}]_2\}\text{Fe}$ (8-Fe^{Et}) in 33% yield. The solution magnetic moment of 8-Fe^{Et} is $5.6 \mu_B$, consistent with an $S = 2$ core with a large spin-orbit contribution.

Only the nacnac components of the coupled PI ligand are bound, leading to two dangling pyridine substituents. No intermediates were detected, nor was the fate of the remaining iron or TMSN_3 determined. It is conceivable that the azide can be acting as a simple donor to trigger the loss of $\text{HN}(\text{TMS})_2$ and form the unsaturated ligand complex $\{\text{Et}(nn)\text{PI}\}^2\text{Fe}^{\text{II}}(\text{N}_3\text{TMS})$, from which coupling and disproportionation ensue. It is also plausible that nitrene transfer does occur, but this ligand could still induce radical character at the pyridine-imine carbon, leading to C–C coupling. Precedent for this possibility comes from Chirik et al.,⁸⁴ who have noted that $(\text{PDI})\text{Fe}=\text{NAr}$ (Ar = bulky aryl) species are best understood as $S = 3/2$ ferric complexes ligated by an imide and the PDI radical anion.

2.4.3. $\{\text{Pr}(nn)\text{PM}\}\text{FeN}(\text{TMS})_2$ (1-Fe^{iPr}) + Ph_2CN_2 . Similar to the preceding section, $\{\text{Pr}(nn)\text{PM}\}\text{FeN}(\text{TMS})_2$ (1-Fe^{iPr}) was treated with Ph_2CN_2 to either induce C–C bond formation or transfer diphenylcarbene, and again the former was discovered, albeit via a pathway that was not anticipated. As Scheme 6 reveals, the addition of diphenyldiazomethane to **1-Fe^{iPr}** afforded a dimer derived from imine carbon–carbon coupling, but a diphenylimino ligand was found attached to each iron center to give $\{\text{Pr}(nn)\text{CHpy}\}_2(\text{FeN}=\text{CPh}_2)_2$ (9-Fe^{iPr}). The reaction conditions— 90°C in benzene for 24 h—suggested a mechanism involving the thermal degradation of Ph_2CN_2 , which is known to generate dinitrogen and $\text{Ph}_2\text{C}=\text{N}=\text{N}=\text{CPh}_2$.⁸⁵ Once the diimine is produced, it can oxidize the Fe(II) center of **1-Fe^{iPr}** to induce $\text{HN}(\text{TMS})_2$ elimination, affording a monomeric $\{\text{Pr}(nn)\text{PI}\}\text{FeN}=\text{CPh}_2$ that has the same spate of $\{\text{Pr}(nn)\text{PI}\}^n$ redox possibilities that were attributed to the precursor to **7-Fe^{iPr}**. The ferrous precursor has radical character at the imine carbon, and coupling at this position provides the product.

2.4.4. Structural Studies of $\{\text{Pr}(nn)\text{CHpy}\}_2\text{Fe}_2\text{Cl}_2$ (7-Fe^{iPr}), $\{\text{[Et}(nn)\text{CHpy}]_2\}\text{Fe}$ (8-Fe^{Et}), and $\{\text{Pr}(nn)\text{CHpy}\}_2(\text{FeN}=\text{CPh}_2)_2$ (9-Fe^{iPr}). Since the products containing new C–C bonds were paramagnetic, their structures were elucidated via single-crystal X-ray crystallography. Data collection and refinement parameters are listed in Table 1, while interatomic distances and angles are given in the captions below each molecular view.

As previously stated, the structure of $\{\text{Pr}(nn)\text{CHpy}\}_2\text{Fe}_2\text{Cl}_2$ (7-Fe^{iPr}) reveals C_2 symmetry, although crystallographically the two units of the dimer are distinct, as the metrics given in

Figure 8 show. The nacnac portions of the coupled ligand are symmetric, but the unique C–C bond has a rather long

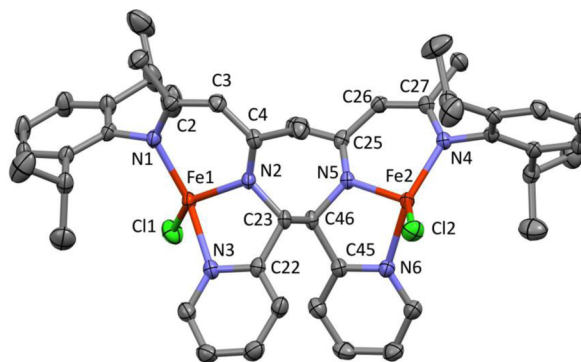


Figure 8. Molecular view of $\{\text{Pr}(nn)\text{CHpy}\}_2\text{Fe}_2\text{Cl}_2$ (7-Fe^{iPr}). Selected interatomic distances (Å) and angles (deg): Fe1–N1, 1.999(2); Fe1–N2, 2.026(2); Fe1–N3, 2.156(2); Fe1–Cl1, 2.248(2); Fe2–N4, 1.984(2); Fe2–N5, 2.025(2); Fe2–N6, 2.133(2); Fe2–Cl2, 2.263(2); N1–C2, 1.342(2); C2–C3, 1.397(3); C3–C4, 1.403(2); N2–C4, 1.328(2); N2–C23, 1.454(2); C22–C23, 1.517(2); N3–C22, 1.353(2); N4–C27, 1.346(2); C26–C27, 1.400(2); C25–C26, 1.410(2); N5–C25, 1.319(2); N5–C46, 1.461(2); C45–C46, 1.521(2); N6–C45, 1.353(3); C23–C46, 1.581(2); N1–Fe1–N2, 91.93(6); N1–Fe1–N3, 141.40(6); N1–Fe1–Cl1, 114.76(5); N2–Fe1–N3, 78.46(6); N2–Fe1–Cl1, 138.04(4); N3–Fe1–Cl1, 95.94(5); N4–Fe2–N5, 92.71(6); N4–Fe2–N6, 136.99(6); N4–Fe2–Cl2, 120.07(5); N5–Fe2–N6, 78.39(6); N5–Fe2–Cl2, 129.92(4); N6–Fe2–Cl2, 96.32(4).

1.581(2) Å distance, a feature previously observed in related systems.³ Each iron(II) has a coordination geometry and bond distances similar to the core of $\{\text{Pr}(nn)\text{PM}\}\text{FeBr}$ (2-Fe^{iPr}), although there is plenty of variation within the angles of each unit. While the nacnac ($91.93(6)^\circ$, $92.71(6)^\circ$) and $\text{N}_{\text{py}}\text{--Fe--N}_{\text{nn}}$ ($78.46(6)^\circ$, $78.39(6)^\circ$) bite angles are quite similar, as are the $\text{N}_{\text{py}}\text{--Fe--Cl}$ angles ($95.94(5)^\circ$, $96.32(4)^\circ$), the $\text{N}_{\text{nn}}\text{--Fe--Cl}$ angles ($114.76(5)^\circ$, $120.07(5)^\circ$; $138.04(4)^\circ$, $129.92(4)^\circ$) show considerable variation, as do the remaining $\text{N}_{\text{nn}}\text{--Fe--N}_{\text{py}}$ angles ($141.40(6)^\circ$ and $136.99(6)^\circ$). Clearly the relatively weak fields in the pseudotetrahedral halves of **7-Fe^{iPr}** are subject to external, that is, packing, as well as internal electronic forces. The diiron distance of $6.003(2)$ Å is not expected to support significant antiferromagnetic coupling,³ but the μ_{eff} of $6.4 \mu_B$, which is less than the expected $6.9 \mu_B$, may reflect some nominal interaction in solution as the average $d(\text{Fe}\cdots\text{Fe})$ may be shorter.

Figure 9 illustrates the mononuclear $\{\text{[Et}(nn)\text{CHpy}]_2\}\text{Fe}$ (8-Fe^{Et}) complex containing two Et(nn)CHpy units coupled and chelating a single Fe(II) center. The compound has C_2 symmetry, with the rotation axis containing the midpoint of the new C–C bond and the iron, although the two halves of the molecule are crystallographically different. The nacnac ligands are coordinated ($d(\text{Fe--N}) = 2.045(12)$ Å ave), and the pyridines dangle off opposing sides of the unique $1.533(7)$ Å C–C bond. While the nacnac bite angles ($89.9(4)^\circ$ ave) and remaining $\text{N}_{\text{nn}}\text{--Fe--N'}_{\text{nn}}$ angles ($141.2(4)^\circ$) are essentially identical, the coupling of the original ligands causes a splay in the complex such that the N1--Fe--N2 angle is $118.4(2)^\circ$, substantially wider than that of N3--Fe--N4 ($81.2(2)^\circ$). The remaining distances are consistent with symmetric bonding within the nacnac halves.

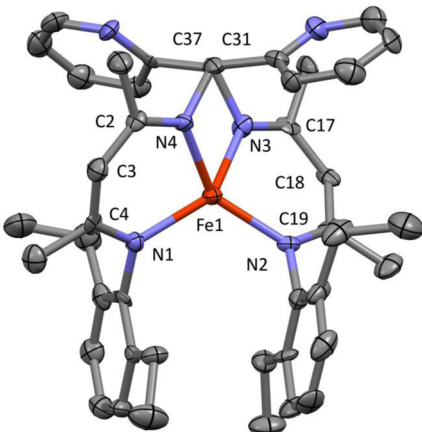


Figure 9. Molecular view of $\{[\text{Et}(\text{nn})\text{CHpy}]_2\}\text{Fe}$ (8- Fe^{Et}). Selected interatomic distances (\AA) and angles (deg): Fe–N1, 2.038(7); Fe–N2, 2.037(7); Fe–N3, 2.042(8); Fe–N4, 2.063(7); N1–C4, 1.339(11); C3–C4, 1.408(13); C2–C3, 1.379(10); N4–C2, 1.316(9); N4–C37, 1.482(11); C31–C37, 1.533(7); N3–C31, 1.466(11); N3–C17, 1.303(10); C17–C18, 1.429(11); C18–C19, 1.381(11); N2–C19, 1.348(10); N1–Fe–N2, 118.4(2); N1–Fe–N3, 141.5(3); N1–Fe–N4, 90.2(3); N2–Fe–N3, 89.6(3); N2–Fe–N4, 140.9(3); N3–Fe–N4, 81.2(2).

Figure 10 depicts $\{\text{iPr}(\text{nn})\text{CHpy}\}_2(\text{FeN}=\text{CPh}_2)_2$ (9- Fe^{iPr}), which exhibits C_i symmetry—both molecular and crystallo-

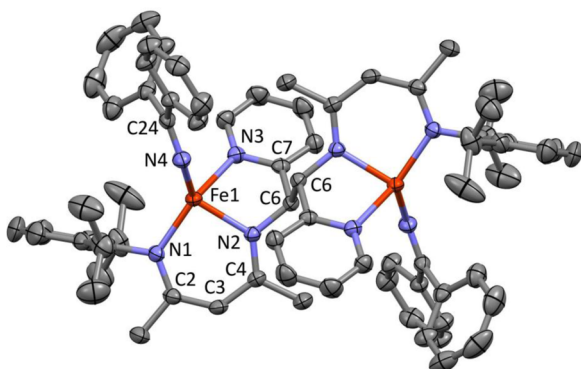


Figure 10. Molecular view of $\{\text{iPr}(\text{nn})\text{CHpy}\}_2(\text{FeN}=\text{CPh}_2)_2$ (9- Fe^{iPr}). Selected interatomic distances (\AA) and angles (deg): Fe–N1, 1.983(2); Fe–N2, 2.011(2); Fe–N3, 2.200(2); Fe–N4, 1.905(2); N1–C2, 1.341(3); C2–C3, 1.391(3); C3–C4, 1.405(3); N2–C4, 1.323(3); N2–C6, 1.454(3); C6–C7, 1.509(3); N3–C7, 1.352(3); N4–C24, 1.260(3); C6–C6', 1.581(4); N1–Fe–N2, 92.81(7); N1–Fe–N3, 133.26(7); N1–Fe–N4, 122.08(7); N2–N3, 77.95(7); N2–Fe–N4, 120.84(7); N3–Fe–N4, 101.09(7); Fe–N4–C24, 140.44(17).

graphic—with its inversion center at the midpoint of the new C–C bond. Metric parameters listed in the caption of Figure 9 are comparable to those of 1- Fe^{iPr} , except that the Fe–N_{nn} distances are somewhat shorter at 1.983(2) and 2.011(2) \AA . The d(C–C) of the unique C–C bond is rather long at 1.581(4),³ but the remaining distances within the ligand framework are normal. The similarity in core angles between 1- Fe^{iPr} and 9- Fe^{iPr} suggest that the disilyl amide and imino ligands have roughly the same perturbation on the system. As in $\{\text{iPr}(\text{nn})\text{CHpy}\}_2\text{Fe}_2\text{Cl}_2$ (7- Fe^{iPr}), the μ_{eff} of 6.5 μ_{B} may indicate some modest antiferromagnetic coupling in solution, but the

d(Fe–Fe) of 6.043 \AA is quite long to facilitate a significant interaction in the solid state.

3. DISCUSSION

3.1. Structures of $\{\text{R}(\text{nn})\text{PM}\}\text{MN}(\text{TMS})_2$ ($\text{R} = \text{iPr}$, $\text{M} = \text{Cr}$ (1- Cr^{iPr}), Fe (1- Fe^{iPr}); $\text{R} = \text{Et}$, $\text{M} = \text{Co}$ (1- Co^{Et})). The metrical parameters regarding $\{\text{R}(\text{nn})\text{PM}\}\text{MN}(\text{TMS})_2$ ($\text{R} = \text{iPr}$, $\text{M} = \text{Cr}$ (1- Cr^{iPr}), Fe (1- Fe^{iPr}); $\text{R} = \text{Et}$, $\text{M} = \text{Co}$ (1- Co^{Et})) clearly show that the deviation away from pseudosquare planar toward tetrahedral occurs for 1- $\text{Co}^{\text{Et}} > 1\text{-Fe}^{\text{iPr}} > 1\text{-Cr}^{\text{iPr}}$. These systems employ relatively weak field ligands; hence, the major factor keeping the coordination geometries near that of square planar is the $\{\text{R}(\text{nn})\text{PM}\}$ chelate, which has bite angles of 78° and 90–92° that contribute significantly toward enforcing a plane about the metal. The remaining bis(trimethylsilyl)amide ligand is the major influence that changes the coordination geometry, and hence the actual metrics are not easily traditionally described.

Neglecting π effects, angular overlap methods (AOMs)⁷⁰ were employed to determine the relative stabilities for each compound, and stabilization energies were calculated for d⁴–d⁷ for each structure and compiled in Figure 11. The usual assumptions were made in the calculations, that is, the radial components pertaining to each structure were considered the same. As expected from standard structure preferences, the pseudosquare planar structure of 1- Cr^{iPr} is preferred for Cr(II) d⁴ by 0.72 e_o over the more distorted structure of 1- Fe^{iPr} and by 0.79 e_o over the most distorted structure, that of 1- Co^{Et} . For the d⁶ and d⁷ configurations, there is really little substantial structural preference for any of the three, with the Fe(II) structure being slightly less likely. As a consequence, the distortion away from the pseudosquare planar geometry by 1- Fe^{iPr} is likely due to slightly improved steric factors and a very small compression of the bond distances, that is, a small change in the radial function. The lowest-energy geometry for 1- Fe^{iPr} is actually the cobalt structure, but in this case it is likely that the isopropyl substituents hamper its formation. The cobalt compound 1- Co^{Et} has ethyl substituents on the aryl ring, and its bond distances are notably shorter, a situation favoring greater radial overlap. Here the Et (vs iPr) steric factor may allow a greater compression of the Co–N bonds, thereby lowering the energy of this configuration, in concert with expected periodic trends.

3.2. Carbonylation Reactions. **3.2.1. Carbonylation of $\{\text{iPr}(\text{nn})\text{PM}\}\text{Fe}^{\text{neoPe}}$ (3- Fe^{iPr}).** Synthesis of $\{\text{iPr}(\text{nn})\text{PM}\}\text{Fe}^{\text{neoPe}}$ (3- Fe^{iPr}) was expected to lead to other derivatives via hydrogenation or exposure to olefins, etc. Clean reactivity was not observed with these substrates, suggesting the desired 1,3-RH elimination of ${}^{\text{neo}}\text{PeH}$, alternatively considered a deprotonation as in cases described by Milstein, de Bruin, and others,^{6,86–88} could not be affected through their addition. Precedent for CO-induced 1,3-elimination existed for $\{\text{nn}-(\text{PM})_2\}\text{FeN}(\text{TMS})_2$ in its conversion to $\{\text{nn}(\text{PM})(\text{PI})\}\text{FeCO}$,⁶ but for 3- Fe^{iPr} , carbonylation led to acyl-carbonyl formation. In the former five-coordinate system,⁶ the CO cannot bind, then insert, since it has to occupy a site trans to the N(TMS)₂ group, and CO insertion into the amide has not been observed. In Scheme 7, the binding of CO generates intermediate $\{\text{iPr}(\text{nn})\text{PM}\}\text{Fe}^{\text{neoPe}}(\text{CO})$, and two options are apparent. The addition of another carbonyl and insertion to form $\{\text{iPr}(\text{nn})\text{PM}\}\text{Fe}(\text{CO}^{\text{neoPe}})\text{CO}$ (4- Fe^{iPr}) trumps 1,3- ${}^{\text{neo}}\text{PeH}$ elimination to produce $\{\text{iPr}(\text{nn})\text{PI}\}\text{Fe}(\text{CO})_2$ (5- Fe^{iPr}). It is conceivable that the geometry of $\{\text{iPr}(\text{nn})\text{PM}\}\text{Fe}^{\text{neoPe}}(\text{CO})$

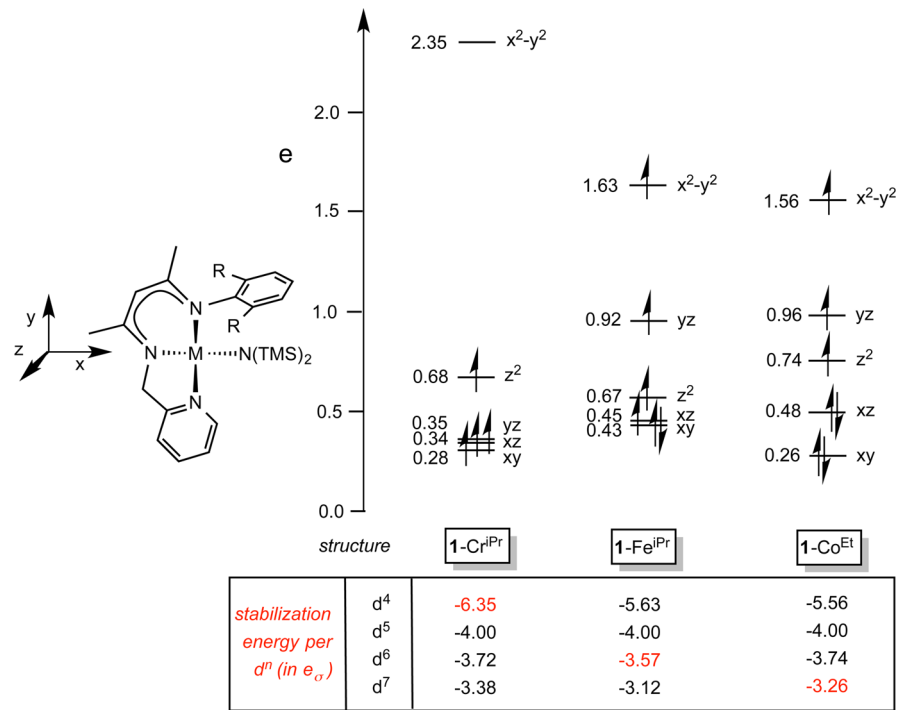
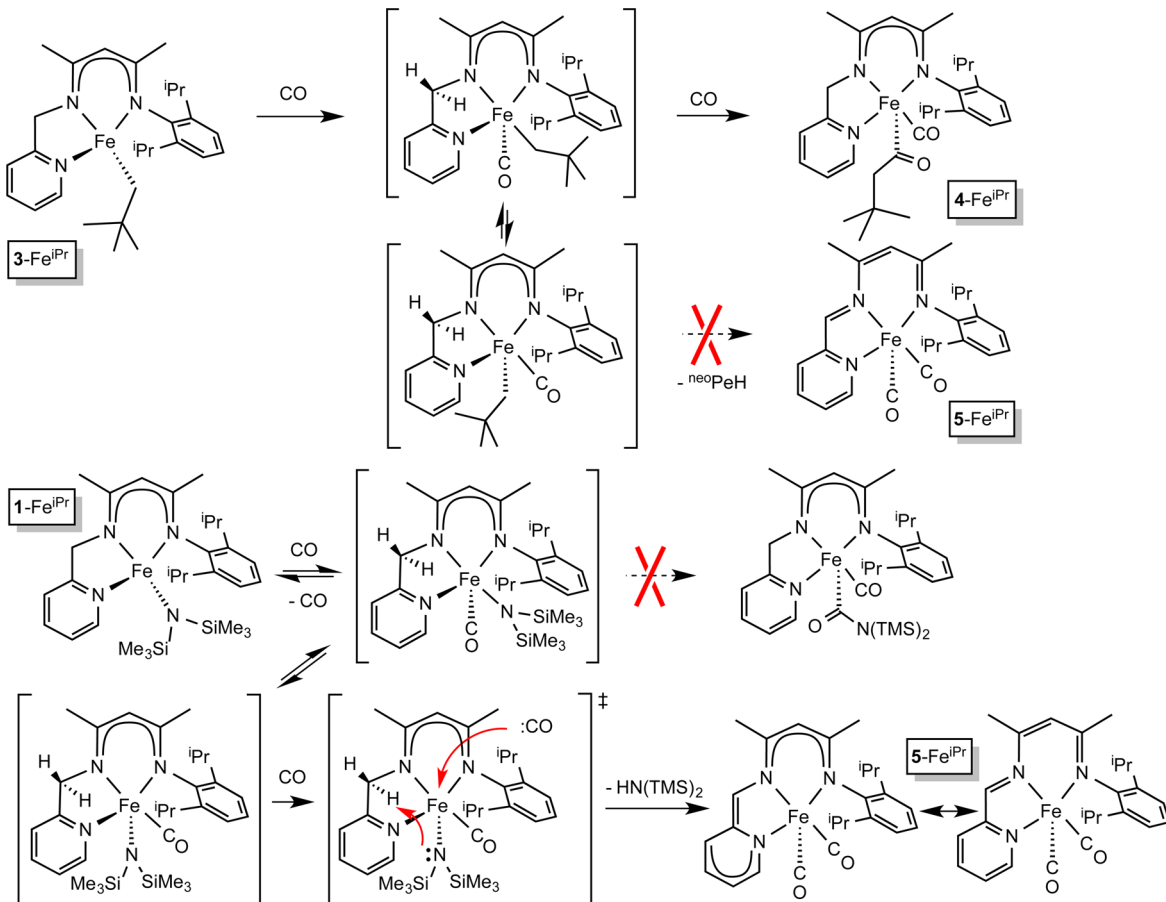


Figure 11. d-Orbital splitting diagrams for $\{R(nn)PM\}MN(TMS)_2$ ($R = iPr$, $M = Cr$ (**1-Cr^{iPr}**), Fe (**1-Fe^{iPr}**); $R = Et$, $M = Co$ (**1-Co^{Et}**)) derived from the angular overlap method. For each compound there are $-8 e_\sigma$ of stabilization due to full occupation of ligand orbitals.

Scheme 7



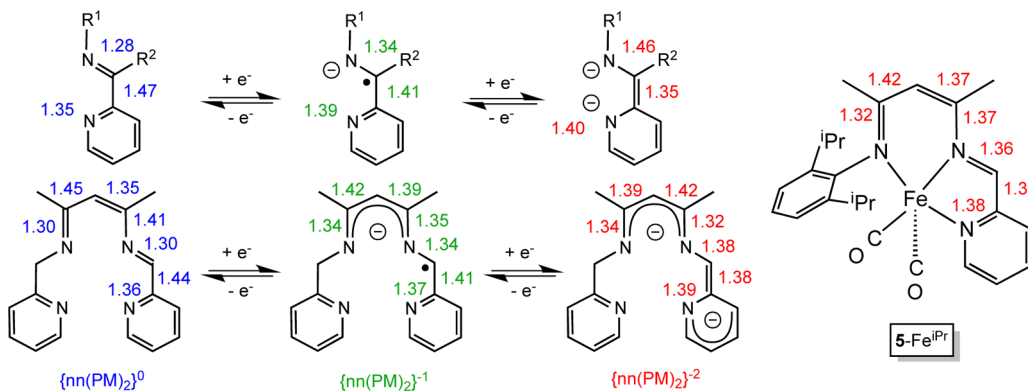


Figure 12. Bond distances for pyridine-imine (PI)ⁿ and {nn(PM)(PI)}ⁿ, determined from structural and calculational data (neutral ($n = 0$, blue), radical anion ($n = -1$, green), and dianion ($n = -2$, red), and bond distances of {ⁱPr(nn)PI}Fe(CO)₂ (5-FeⁱPr).

affects the course of reactivity, since a basal ^{neo}Pe group cannot reach the PM arm of the chelate to deprotonate it, yet a migratory insertion is feasible.

3.2.2. Formation and Structural Parameters of $\{^i\text{Pr}(\text{nn})-\text{PI}\}\text{Fe}(\text{CO})_2$ (5-Fe $^{i\text{Pr}}$**).** Unlike the $^{\text{neo}}\text{Pe}$ -derivative, $\{^i\text{Pr}(\text{nn})\text{PM}\}-\text{FeN}(\text{TMS})_2$ (**1-Fe $^{i\text{Pr}}$**), like its $\{\text{nn}(\text{PM})_2\}\text{FeN}(\text{TMS})_2$ predecessor,⁶ undergoes 1,3-HN(TMS)₂ elimination^{86,87} in the presence of CO to afford $\{^i\text{Pr}(\text{nn})\text{PI}\}\text{Fe}(\text{CO})_2$ (**5-Fe $^{i\text{Pr}}$**). Insertion of CO into the amide is less likely to be an alternative route; hence, elimination occurs to produce the dicarbonyl. It is also plausible that the lone pair on the amide has a favorable orientation for deprotonation of the chelate PM arm, in contrast to a $^{\text{neo}}\text{Pe}$ group, thereby utilizing a lower barrier for 1,3-elimination.

Figure 12 illustrates the chelate bond distances of $\{\text{Pr}(\text{nn})\text{PI}\}\text{Fe}(\text{CO})_2$ (**5-Fe^{iPr}**) in comparison to the previously studied pyridine-imine (PI) bidentate chelate^{7,53,54} and the tetradentate chelate, $\{\text{nn}(\text{PM})(\text{PI})\}^n$ ($n = 0, -1, -2$).⁶ The PI metrics for various redox states of the ligand are well-established, and while there are limited examples of complexes containing the $\{\text{nn}(\text{PM})(\text{PI})\}^n$ ligand, there is decent correspondence between experiment and theory; hence, the numbers are likely to be sufficiently viable. Note that comparative distances for **5-Fe^{iPr}** are ambiguous enough to render the redox assignment difficult. The PI arm has values close to $n = -2$ for the tetradentate, but as the tridentate chelate is traversed, the bond lengths tend toward $n = -1$, and eventually the final $d(\text{NC}) = 1.32 \text{ \AA}$ is nearly that expected of the neutral ligand. A case can certainly be made for a $\{\text{Pr}(\text{nn})\text{PI}\}^-$ radical anion antiferromagnetically coupled to a low-spin Fe(I) center, or a dianion, $\{\text{Pr}(\text{nn})\text{PI}\}^{2-}$, bound to a low spin Fe(II) species. Since the chelate in **4-Fe^{iPr}** is monoanionic, it is tempting to assign a -1 redox state to the $\{\text{Pr}(\text{nn})\text{PI}\}^-$ ligand in **5-Fe^{iPr}**. Alternatively, the ferrous state of **4-Fe^{iPr}** suggests that the similar metrics of **5-Fe^{iPr}** also may be indicative of Fe(II).

3.2.3. Calculation of $\{^i\text{Pr}(\text{nn})\text{PI}\}\text{Fe}(\text{CO})_2$ ($5\text{-Fe}^{i\text{Pr}}$). Figure 13 shows the calculated geometry of $\{^i\text{Pr}(\text{nn})\text{PI}\}\text{Fe}(\text{CO})_2$, ($5\text{-Fe}^{i\text{Pr}}$), including chelate bond distances that are each within 0.02 Å of the crystallographic bond lengths listed in Figure 6. According to the metrics in Figure 12, the tridentate chelate $\{^i\text{Pr}(\text{nn})\text{PI}\}^{2-}$ is best considered a dianionic ligand, albeit with some subtle differences as outlined above. Furthermore, the metrics of $5\text{-Fe}^{i\text{Pr}}$ are close to those of hypothetical $\{^i\text{Pr}(\text{nn})\text{PI}\}\text{Mg}$, which can be considered a prototypical dianion chelated to Mg^{2+} . Although the CO stretching frequencies of the dicarbonyls ($5\text{-Fe}^{i\text{Pr}}$, 1910, 1971 cm $^{-1}$; 5-Fe^{Et} , 1909, 1960

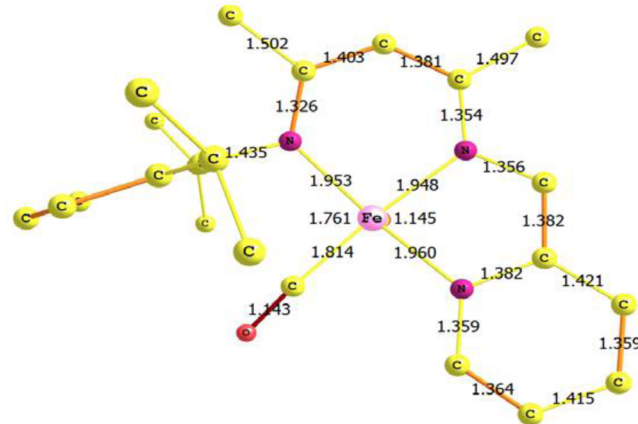


Figure 13. Calculated structure of $\{\text{Pr}(\text{nn})\text{PI}\}\text{Fe}(\text{CO})_2$ (**5-Fe^{iPr}**) showing pertinent bond lengths most consistent with a dianionic $\{\text{Pr}(\text{nn})\text{PI}\}^{2-}$ ligand.

cm^{-1}) are somewhat low for Fe(II), the $\{\text{R}(\text{nn})\text{PI}\}^{2-}$ chelate is not a competitive π -acid ligand, and the d^6 configuration effectively backbonds into the π^* orbitals of the two carbonyls.

The orbitals that comprise the ligand field and those related to the tridentate chelate are not so easily discerned in $\{\text{Pr}(\text{nn})\text{P}\}\text{Fe}(\text{CO})_2$ (**5-Fe^{I_{Pr}}**), as Figure 14 illustrates. Because of the low symmetry and the similar relative energies of the d_{z²}, ligand- π^b , and ligand- π^* orbitals, it is difficult to designate the major components. Assigning a particular d orbital to a depiction is challenging, and identification of a classical "ligand field" is not possible as the d orbitals—in particular the σ^* orbitals (i.e., d_{x²-y²} and d_{z²})—are so mixed that they are spread over several molecular orbitals.

Figure 14 shows 12 e⁻ occupying six orbitals of mixed composition at relatively low energies, three of which can be roughly assigned as the d_{xy} (-7.22 eV), d_{xz} (-7.42 eV), and d_{yz} (-6.18 eV) orbitals. While the remaining three in this region of energy definitely have major aryl π^b components, there is no denying significant d orbital character in each. The dominant depiction in the figure is of the highest occupied molecular orbital (HOMO), which is an orbital that is essentially pyridine-imine π^* , with a small component of d_{z²} (~20%). Occupation of this orbital leads to the conclusion that the tridentate ligand is a dianion, as the metric parameters implied. The remaining unoccupied orbitals testify to the dispersed d character in the σ antibonding orbitals.

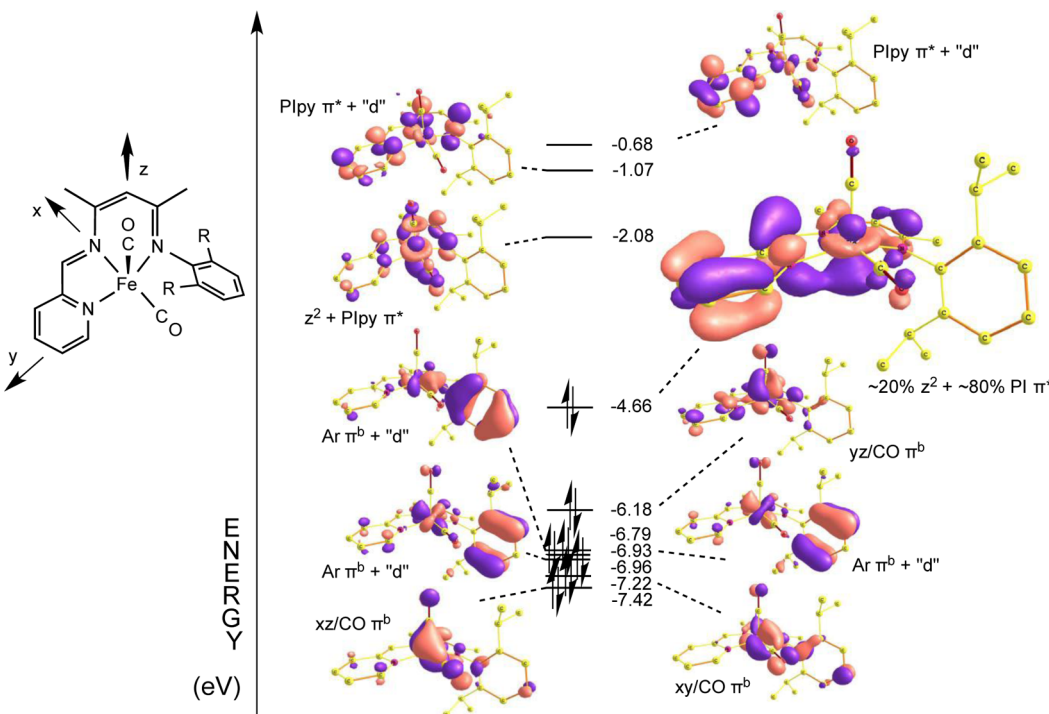


Figure 14. Truncated molecular orbital diagram of $\{\text{Pr}(\text{nn})\text{PI}\}\text{Fe}(\text{CO})_2$ (**5-Fe^{Pr}**) showing highly admixed d/ligand orbitals. The enlarged orbital is that of the HOMO, which is largely (~80%) ligand-based, consistent with a dianionic $\{\text{Pr}(\text{nn})\text{PI}\}^{2-}$ ligand. Higher orbitals show little d character, as the σ^* contributions of $d_{x^2-y^2}$ and the remainder of d_{z^2} are spread over several orbitals in this low-symmetry environment, making it difficult to even identify the ligand field.

3.2.4. Carbonylation of $\{^i\text{Pr}(\text{nn})\text{PM}\}\text{CrN}(\text{TMS})_2$ (1-Cr^{iPr}**).** As Scheme 3 proclaims, carbonylation of $\{^i\text{Pr}(\text{nn})\text{PM}\}\text{CrN}(\text{TMS})_2$ (**1-Cr^{iPr}**) did not produce an analogue to $\{^i\text{Pr}(\text{nn})\text{PI}\}\text{Fe}(\text{CO})_2$ (**5-Fe^{iPr}**) via deamination. Instead, migration of the aryl-nitrogen arm of the nacnac to the imine carbon ensued to afford a pyrimidine-pyridine ligand bound to a chromium tetracarbonyl, $\{\kappa^2\text{-N,N-pyrim-pyr}\}\text{Cr}(\text{CO})_4$ (**6-Cr^{iPr}**). It is likely that the $\{^i\text{Pr}(\text{nn})\text{PI}\}^n$ ligand on putative intermediate $\{^i\text{Pr}(\text{nn})\text{-PI}\}\text{Cr}(\text{CO})_3$ is neutral ($n = 0$), since an anion (13 e^-) or dianion (14 e^-) would be less susceptible to nucleophilic attack at the imine carbon. Withdrawal of electron density upon carbonylation may render the chromium center “oxidized” via π backbonding and therefore incapable of reducing the ligand. Cyclization then occurs just as in the free organic species generated via oxidation of the dianion.

3.2.5. Calculation of Putative $\{^i\text{Pr}(\text{nn})\text{PI}\}\text{Cr}(\text{CO})_3$. A likely precursor to $\{\kappa^2-\text{N},\text{N}-\text{pyrim-pyr}\}\text{Cr}(\text{CO})_4$ ($6\text{-Cr}^{i\text{Pr}}$) in the deamination of $\{^i\text{Pr}(\text{nn})\text{PM}\}\text{CrN}(\text{TMS})_2$ ($1\text{-Cr}^{i\text{Pr}}$) is the tricarbonyl complex $\{^i\text{Pr}(\text{nn})\text{PI}\}\text{Cr}(\text{CO})_3$. Figure 15 reveals the chelate bond distances in the calculated precursor, and the metrical parameters are clearly those of a neutral ligand, especially when compared to the structures of $\{^i\text{Pr}(\text{nn})\text{PI}\}\text{Li}$ and $\{^i\text{Pr}(\text{nn})\text{PI}\}\text{Mg}$ computed at the same level of theory. The calculations thus buttress the argument that the 12 e^- neutral ligand, just like its unbound form, is unstable and susceptible to cyclization. Furthermore, the ligand field of $\{^i\text{Pr}(\text{nn})\text{PI}\}\text{Cr}(\text{CO})_3$ contains a “ t_{2g} ” set of filled orbitals (HOMO, HOMO-1, HOMO-2) that manifest backbonding to the carbonyls. No filled ligand π^* orbitals are observed in the same region of energy, and hence the neutral description of the $\{^i\text{Pr}(\text{nn})\text{PI}\}$ ligand appears apt.

3.3. Carbon–Carbon Bond-Forming Reactions.

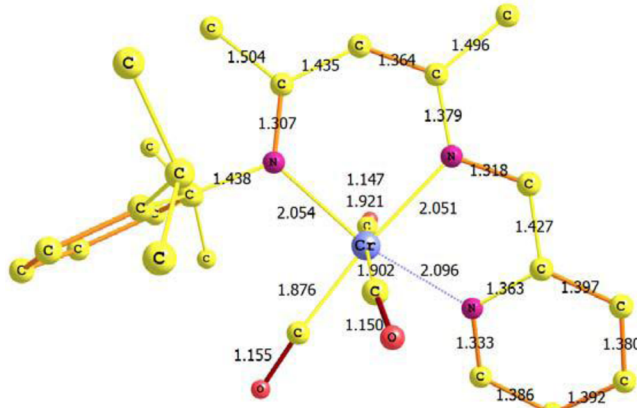


Figure 15. Calculated structure of putative $\{\text{Pr}(\text{nn})\text{PI}\}\text{Cr}(\text{CO})_3$ showing pertinent bond lengths most consistent with a neutral $\{\text{Pr}(\text{nn})\text{PI}\}$ ligand.

Chloride. Ferric species have a history of oxidative coupling chemistry,^{82,83} and formation of $\{\text{Pr}(\text{nn})\text{CH}(\text{py})\}_2\text{Fe}_2\text{Cl}_2$ (7- $\text{Fe}^{i\text{Pr}}$) from $[\{\text{Pr}(\text{nn})\text{PI}\}^{2-}] (\text{K}^+(\text{THF})_x)_2$ and FeCl_3 affords a classic look at this process. As Scheme 4 alludes, the formation of the desired $[\{\text{Pr}(\text{nn})\text{PI}\}^{2-}] \text{FeCl}$ monomer should induce a formal 1 e^- reduction to $\text{Fe}(\text{II})$, which generates radical character at the imine, leading to simple C–C bond formation. The process is reminiscent of how transition metals, especially iron(III), are thought to oxidize phenol or phenoxide.^{89,90,91} Formation of $(\text{PhO})\text{Fe}^{\text{III}}\text{X}_2$ leads to $(\text{PhO}-)\text{Fe}^{\text{II}}\text{X}_2$, and coupling adjacent to the phenoxide bond, or para to the phenoxide, occurs in like fashion, followed by proton transfer to regenerate the phenol.

3.3.2. Oxidation of $\{\text{Pr}(\text{nn})\text{PM}\}\text{FeN}(\text{TMS})_2$ (1-Fe^{iPr}**) by $\text{Ph}_2\text{C}=\text{N}\cdot$ Radical.** The generation of $\{\text{iPr}(\text{nn})\text{-CHpy}\}_2(\text{FeN}=\text{CPh}_2)_2$ (**9-Fe^{iPr}**) has a plausible mechanism in common with that of **7-Fe^{iPr}**, as is illustrated in Scheme 6. No formation of the dimer was indicated unless the reaction was carried out at temperatures known to decompose Ph_2CN_2 to dinitrogen and $1/2 \text{Ph}_2\text{C}=\text{N}-\text{N}=\text{CPh}_2$.⁸⁵ The subsequent oxidation of precursor $\{\text{Pr}(\text{nn})\text{PM}\}\text{FeN}(\text{TMS})_2$ (**1-Fe^{iPr}**) by $\text{Ph}_2\text{C}=\text{N}\cdot$ radical is likely to induce deamination, but the resulting $[\{\text{Pr}(\text{nn})\text{PM}\}^{2-}] \text{Fe}-\text{N}=\text{CPh}_2$ is still Fe(III), just as $[\{\text{Pr}(\text{nn})\text{PI}\}^{2-}] \text{FeCl}$ was similarly viewed above. As postulated for **7-Fe^{iPr}**, a formal 1e^- reduction to Fe(II) enables carbon–carbon coupling at the imine carbon, leading to the dimer **9-Fe^{iPr}**.

3.3.3. Carbon–Carbon Bond Formation and Disproportionation: $\{[\text{Et}(\text{nn})\text{CHpy}]_2\}\text{Fe}$ (8-Fe^{Et}**).** Scheme 5 illustrates a reasonable path toward $\{[\text{Et}(\text{nn})\text{CHpy}]_2\}\text{Fe}$ (**8-Fe^{Et}**) involving the degradation of TMSN_3 , which can serve as a simple donor to trigger deamination of $\{\text{Et}(\text{nn})\text{PM}\}\text{FeN}(\text{TMS})_2$ (**1-Fe^{Et}**) and as an oxidant via nitrene transfer. An intermediate such as $[\{\text{Et}(\text{nn})\text{PI}\}^n] \text{Fe}=\text{NTMS}$ can be Fe(II) if $n = 0$, Fe(III) if $n = -1$, or Fe(IV) if $n = -2$ (not shown). Precedent from Chirik's work⁸⁴ suggests that the ferric state can also lead to radical character at the imine carbon and to formation of the new C–C bond via coupling. The direct product of that coupling would be $[\{\text{Et}(\text{nn})\text{CHpy}\}_2](\text{Fe}=\text{NTMS})_2$, and the iron centers would still be Fe(III). All prior examples involving the nacnac-based chelates suggest that this is an intrinsically unstable redox environment, perhaps prompting the disproportionation to afford the stable Fe(II) product $\{[\text{Et}(\text{nn})\text{CHpy}]_2\}\text{Fe}$ (**8-Fe^{Et}**) and some unknown complementary iron/nitrene byproduct(s).

4. CONCLUSIONS

On the basis of previous efforts pertaining to tetradentate chelates $\{\text{Me}_2\text{C}(\text{CH}_2\text{N}=\text{CHpy})_2\}^n$ ($n = 0, -1, -2, -3, -4$),⁷ $\{\text{nacnac}(\text{CH}_2\text{py})_2\}^-$, and $\{\text{nacnac}(\text{CH}_2\text{py})(\text{CHpy})\}^n$,⁶ a switch to tridentate chelates was considered to increase the possibility of metal-centered reactivity, or C–X or C–C bond-forming processes at the coordinated ligand. Replacement of the PI (or PM) arm of the aforementioned nacnac-based ligands led to the synthesis and application of $\{\text{R}(\text{nn})\text{PM}\}^-$ and $\{\text{R}(\text{nn})\text{PI}\}^n$ ($n = 0, -2$), where R is a 2,6-di-R-substituted phenyl residue. As a consequence, reactivity at the ligand was enhanced, leading to several C–C and one C–N bond-forming process. In every case, the reactivity appears to stem from an oxidized ($4n$) or monoreduced ligand rather than one with a stable $4n + 2$ π -electron configuration,⁹² as was previously postulated.⁶ It is proposed that the ability to transiently stabilize $4n$ π -electron configurations is critical to the application of redox non-innocence to productive chemical reactivity, either in catalysis or in stoichiometric transformations.

5. EXPERIMENTAL SECTION

Since the Figures and Schemes provide reasonable experimental details, the full experimental methods were deposited as Supporting Information.

ASSOCIATED CONTENT

Supporting Information

Full experimental details, including procedures, X-ray structural details, Mössbauer acquisition information, and calculation-

al^{93–95} techniques. This material is available free of charge via the Internet at <http://pubs.acs.org>.

AUTHOR INFORMATION

Corresponding Author

*E-mail: ptw2@cornell.edu. Fax: 607 255 4173.

Notes

The authors declare no competing financial interest.

ACKNOWLEDGMENTS

P.T.W. thanks the U.S. National Science Foundation (NSF) (CHE-1055505) and Cornell University, and T.R.C. thanks the NSF (CHE-1057758) for financial support.

REFERENCES

- Frazier, B. A.; Wolczanski, P. T.; Lobkovsky, E. B. *Inorg. Chem.* **2009**, *48*, 11576–11585.
- (a) Frazier, B. A.; Bartholomew, E. R.; Wolczanski, P. T.; DeBeer, S.; Santiago-Berrios, M.; Abruna, H. D.; Lobkovsky, E. B.; Bart, S. C.; Mossin, S.; Meyer, K.; Cundari, T. R. *Inorg. Chem.* **2011**, *50*, 12414–12436. (b) Frazier, B. A.; Wolczanski, P. T.; Lobkovsky, E. B.; Cundari, T. R. *J. Am. Chem. Soc.* **2009**, *131*, 3428–3429.
- (3) Frazier, B. A.; Williams, V. A.; Wolczanski, P. T.; Bart, S.; Meyer, K.; Cundari, T. R.; Lobkovsky, E. B. *Inorg. Chem.* **2013**, *52*, 3295–3312.
- (4) Frazier, B. A.; Wolczanski, P. T.; Keresztes, I.; DeBeer, S.; Lobkovsky, E. B.; Pierpont, A. W.; Cundari, T. R. *Inorg. Chem.* **2012**, *51*, 8177–8186.
- (5) Hulley, E. B.; Wolczanski, P. T.; Lobkovsky, E. B. *J. Am. Chem. Soc.* **2011**, *133*, 18058–18061.
- (6) Williams, V. A.; Wolczanski, P. T.; Sutter, J.; Meyer, K.; Lobkovsky, E. B.; Cundari, T. R. *Inorg. Chem.* **2014**, *53*, 4459–4474.
- (7) Williams, V. A.; Hulley, E. B.; Wolczanski, P. T.; Lancaster, K. M.; Lobkovsky, E. B. *Chem. Sci.* **2013**, *4*, 3636–3648.
- (8) Jiao, R.; Shen, X. D.; Xue, M. Q.; Zhang, Y.; Yao, Y. M.; Shen, Q. *Chem. Commun.* **2010**, *46*, 4118–4120.
- (9) Holland, P. L. *Acc. Chem. Res.* **2008**, *41*, 905–914.
- (10) (a) Smith, J. M.; Sadique, A. R.; Cundari, T. R.; Rodgers, K. R.; Lakat-Rodgers, G.; Lachicotte, R. J.; Flaschenriem, C. J.; Vela, J.; Holland, P. L. *J. Am. Chem. Soc.* **2006**, *128*, 756–769. (b) Smith, J. M.; Lachicotte, R. J.; Pittard, K. A.; Cundari, T. R.; Lukat-Rodgers, G.; Rodgers, K. R.; Holland, P. L. *J. Am. Chem. Soc.* **2001**, *123*, 9222–9223.
- (11) (a) Holland, P. L.; Cundari, T. R.; Perez, L. L.; Eckert, N. A.; Lachicotte, R. J. *J. Am. Chem. Soc.* **2002**, *124*, 14416–14424. (b) Andres, H.; Bominara, E. L.; Smith, J. M.; Eckert, N. A.; Holland, P. L.; Munck, E. *J. Am. Chem. Soc.* **2002**, *124*, 3012–3025.
- (12) (a) Cowley, R. E.; Eckert, N. A.; Vaddadi, S.; Figg, T. M.; Cundari, T. R.; Holland, P. L. *J. Am. Chem. Soc.* **2011**, *133*, 9796–9811. (b) Eckert, N. A.; Vaddadi, S.; Stoian, S.; Lachicotte, R. J.; Cundari, T. R.; Holland, P. L. *Angew. Chem., Int. Ed.* **2006**, *45*, 6868–6871. (c) Cowley, R. E.; Holland, P. L. *Inorg. Chem.* **2012**, *51*, 8352–8361.
- (13) Yu, Y.; Sadique, A. R.; Smith, J. M.; Dugan, T. R.; Cowley, R. E.; Brennessel, W. W.; Flaschenriem, C. J.; Bill, E.; Cundari, T. R.; Holland, P. L. *J. Am. Chem. Soc.* **2008**, *130*, 6624–6638.
- (14) (a) Vela, J.; Smith, J. M.; Yu, Y.; Ketterer, N. A.; Flaschenriem, C. J.; Lachicotte, R. J.; Holland, P. L. *J. Am. Chem. Soc.* **2005**, *127*, 7857–7870. (b) Dugan, T. R.; Goldberg, J. M.; Brennessel, W. W.; Holland, P. L. *Organometallics* **2012**, *31*, 1349–1360.
- (15) (a) Dugan, T. R.; Bill, E.; MacLeod, K. C.; Christian, G. J.; Cowley, R. E.; Brennessel, W. W.; Ye, S. F.; Neese, F.; Holland, P. L. *J. Am. Chem. Soc.* **2012**, *134*, 20352–20364. (b) Cowley, R. E.; Golder, M. R.; Eckert, N. A.; Al-Afayouni, M. H.; Holland, P. L. *Organometallics* **2013**, *32*, 5289–5298.

- (16) (a) Rodriguez, M. M.; Bill, E.; Brennessel, W. W.; Holland, P. L. *Science* **2011**, *334*, 780–783. (b) Chiang, K. P.; Bellows, S. M.; Brennessel, W. W.; Holland, P. L. *Chem. Sci.* **2014**, *5*, 267–274.
- (17) (a) Wiese, S.; McAfee, J. L.; Pahls, D. R.; McMullin, C. L.; Cundari, T. R.; Warren, T. H. *J. Am. Chem. Soc.* **2012**, *134*, 10114–10121. (b) Kogut, E.; Wiencko, H. L.; Zhang, L. B.; Cordeau, D. E.; Warren, T. J. *J. Am. Chem. Soc.* **2005**, *127*, 11248–11249. (c) Kogut, E.; Zeller, A.; Warren, T. H.; Strassner, T. *J. Am. Chem. Soc.* **2004**, *126*, 11984–11994.
- (18) (a) Gephart, R. T.; Huang, D. L.; Aguila, M. J. B.; Schmidt, G.; Shahu, A.; Warren, T. H. *Angew. Chem., Int. Ed.* **2012**, *51*, 6488–6492. (b) Badei, Y. M.; Krishnaswamy, A.; Melzer, M. M.; Warren, T. H. *J. Am. Chem. Soc.* **2006**, *128*, 15056–15057. (c) Dai, X. L.; Warren, T. H. *J. Am. Chem. Soc.* **2004**, *126*, 10085–10094. (d) Gephart, R. T.; McMullin, C. L.; Sapiezynski, N. G.; Jang, E. S.; Aguila, M. J. B.; Cundari, T. R.; Warren, T. H. *J. Am. Chem. Soc.* **2012**, *134*, 17350–17353.
- (19) Dai, X. L.; Kapoor, P.; Warren, T. H. *J. Am. Chem. Soc.* **2004**, *126*, 4798–4799.
- (20) Mindiola, D. *J. Acc. Chem. Res.* **2006**, *39*, 813–821.
- (21) Mindiola, D. *J. Angew. Chem., Int. Ed.* **2009**, *48*, 6198–6200.
- (22) (a) Tran, B. L.; Washington, M. P.; Henckel, D. A.; Gao, X. F.; Park, H.; Pink, M.; Mindiola, D. *J. Chem. Commun.* **2012**, 1529–1531. (b) Bailey, B. C.; Basuli, F.; Huffman, J. C.; Mindiola, D. *J. Organometallics* **2006**, *25*, 3963–3968. (c) Kilgore, U. J.; Basuli, F.; Huffman, J. C.; Mindiola, D. J. *Inorg. Chem.* **2006**, *45*, 487–489. (d) Basuli, F.; Aneetha, H.; Huffman, J. C.; Mindiola, D. J. *J. Am. Chem. Soc.* **2005**, *127*, 17992–17993. (e) Zhao, G. Y.; Basuli, F.; Kilgore, U. J.; Fan, H. J.; Aneetha, H.; Huffman, J. C.; Wu, G.; Mindiola, D. *J. J. Am. Chem. Soc.* **2006**, *128*, 13575–13585.
- (23) Adhikari, D.; Basuli, F.; Orlando, J. H.; Gao, X. F.; Huffman, J. C.; Pink, M.; Mindiola, D. *J. Organometallics* **2009**, *28*, 4115–4125.
- (24) (a) Tran, B. L.; Singhal, M.; Park, H.; Lam, O. P.; Pink, M.; Krzystek, J.; Ozarowski, A.; Telser, J.; Meyer, K.; Mindiola, D. *J. Angew. Chem., Int. Ed.* **2010**, *49*, 9871–9875. (b) Tran, B. L.; Pinter, B.; Nichols, A. J.; Konopka, F. T.; Thompson, R.; Chen, C. H.; Krzystek, J.; Ozarowski, A.; Telser, J.; Baik, M. H.; Meyer, K.; Mindiola, D. *J. J. Am. Chem. Soc.* **2012**, *134*, 13035–13045.
- (25) Fan, H. J.; Adhikari, D.; Saleh, A. A.; Clark, R. L.; Zuno-Cruz, F. J.; Cabrera, G. S.; Huffman, J. C.; Pink, M.; Mindiola, D. J.; Baik, M. H. *J. Am. Chem. Soc.* **2008**, *130*, 17351–17361.
- (26) MacAdams, L. A.; Kim, W. K.; Liable-Sands, L. M.; Guzei, I. A.; Rheingold, A. L.; Theopolis, K. H. *Organometallics* **2002**, *21*, 952–960.
- (27) (a) Kim, W. K.; Fevola, M. J.; Liable-Sands, L. M.; Rheingold, A. L.; Theopolis, K. H. *Organometallics* **1998**, *17*, 4541–4543. (b) MacAdams, L. A.; Buffone, G. P.; Incarvito, C. D.; Rheingold, A. L. *J. Am. Chem. Soc.* **2005**, *127*, 1082–1083. (c) Monillas, W. H.; Young, J. F.; Yap, G. P. A.; Theopolis, K. H. *Dalton Trans.* **2013**, *42*, 9198–9210 (d).
- (28) (a) Monillas, W. H.; Yap, G. P. A.; MacAdams, L. A.; Theopolis, K. H. *J. Am. Chem. Soc.* **2007**, *129*, 8090–8091. (b) Dai, F.; Yap, G. P. A.; Theopolis, K. H. *J. J. Am. Chem. Soc.* **2013**, *135*, 16774–16776. (c) Monillas, W. H.; Yap, G. P. A.; Theopolis, K. H. *Inorg. Chim. Acta* **2011**, *369*, 103–119.
- (29) (a) Monillas, W. H.; Yap, G. P. A.; Theopolis, K. H. *Angew. Chem., Int. Ed.* **2007**, *46*, 6692–6694. (b) Benard, M.; Rohmer, M. M.; Lopez, X.; Theopolis, K. H. *Angew. Chem., Int. Ed.* **2008**, *47*, 5597–5599. (c) MacAdams, L. A.; Buffone, G. P.; Incarvito, C. D.; Golen, J. A.; Rheingold, A. L.; Theopolis, K. H. *Chem. Commun.* **2003**, 1164–1165.
- (30) Whitehorne, T. J. J.; Schaper, F. *Inorg. Chem.* **2013**, *52*, 13612–13622.
- (31) Gupta, A. K.; Tolman, W. B. *Inorg. Chem.* **2012**, *51*, 1881–1888.
- (32) (a) Chang, K. C.; Lu, C. F.; Wang, P. Y.; Lu, D. Y.; Chen, H. Z.; Kuo, T. S.; Tsai, Y. C. *Dalton Trans.* **2011**, *40*, 2324–2331. (b) Lin, K. M.; Wang, P. Y.; Shieh, Y. J.; Chen, H. Z.; Kuo, T. S.; Tsai, Y. C. *New J. Chem.* **2010**, *34*, 1737–1745.
- (33) Tonsetich, Z. J.; Heroquel, F.; Do, L. H.; Lippard, S. J. *Inorg. Chem.* **2011**, *50*, 1570–1579.
- (34) (a) Zhou, W.; Tang, L. M.; Patrick, B. O.; Smith, K. M. *Organometallics* **2011**, *30*, 603–610. (b) Chapouret, Y.; MacLeod, K. C.; Baisch, U.; Patrick, B. O.; Smith, K. M.; Poli, R. *Organometallics* **2010**, *29*, 167–176.
- (35) El-Zoghbi, I.; Kebdani, M.; Whitehorne, T. J. J.; Schaper, F. *Organometallics* **2013**, *32*, 6986–6995.
- (36) (a) Gianetti, T. L.; Nocton, G.; Minasian, S. G.; Tomson, N. C.; Kilcoyne, A. L. D.; Kozimor, S. A.; Shuh, D. K.; Tyliszczak, T.; Bergman, R. G.; Arnold, J. *J. Am. Chem. Soc.* **2013**, *135*, 3224–3236. (b) Gianetti, T. L.; Bergman, R. G.; Arnold, J. *J. Am. Chem. Soc.* **2013**, *135*, 8145–8148. (c) Gianetti, T. L.; Tomson, N. C.; Arnold, J.; Bergman, R. G. *J. Am. Chem. Soc.* **2011**, *133*, 14904–14907. (d) Tomson, N. C.; Arnold, J.; Bergman, R. G. *Organometallics* **2010**, *29*, 5010–5025. (e) Tomson, N. C.; Arnold, J.; Bergman, R. G. *Organometallics* **2010**, *29*, 2926–2942. (f) Tomson, N. C.; Arnold, J.; Bergman, R. G. *Dalton Trans.* **2011**, *40*, 7718–7729.
- (37) (a) Hadzovic, A.; Song, D. T. *Inorg. Chem.* **2008**, *47*, 12010–12017. (b) Annibale, V. T.; Tan, R. Y.; Janetzko, J.; Lund, L. M.; Song, D. T. *Inorg. Chim. Acta* **2012**, *380*, 308–321.
- (38) (a) Phillips, A. D.; Thommes, K.; Scopelliti, R.; Gandolfi, C.; Albrecht, M.; Severin, K.; Schreiber, D. F.; Dyson, P. J. *Organometallics* **2011**, *30*, 6119–6132. (b) Phillips, A. D.; Zava, O.; Scopelliti, R.; Nazarov, A. A.; Dyson, P. J. *Organometallics* **2010**, *29*, 417–427.
- (39) Tsai, Y. C. *Coord. Chem. Rev.* **2012**, *256*, 722–758.
- (40) Yao, S. L.; Driess, M. *Acc. Chem. Res.* **2012**, *45*, 276–287.
- (41) Marshak, M. P.; Chambers, M. B.; Nocera, D. G. *Inorg. Chem.* **2012**, *51*, 11190–11197.
- (42) Khusniyarov, M. M.; Bill, E.; Weyhermüller, T.; Bothe, E.; Wieghardt, K. *Angew. Chem., Int. Ed.* **2011**, *50*, 1652–1655.
- (43) (a) Hope, J. M.; Wilson, J. J.; Lippard, S. J. *Dalton Trans.* **2013**, *42*, 3176–3180. (b) Marlier, E. E.; Sadowsky, D.; Cramer, C. J.; McNeill, K. *Inorg. Chim. Acta* **2011**, *369*, 173–179.
- (44) Marlier, E. E.; Ulrich, B. A.; McNeill, K. *Inorg. Chem.* **2012**, *51*, 2079–2085.
- (45) Jørgensen, C. K. *Helv. Chim. Acta* **1967**, *50* (Supp. 1), 131–146.
- (46) Pierpont, C. G. *Coord. Chem. Rev.* **2001**, *216*, 99–125.
- (47) Evangelio, E.; Ruiz-Molina, D. *Eur. J. Inorg. Chem.* **2005**, 2957–2971.
- (48) Ray, K.; Petrenko, T.; Wieghardt, K.; Neese, F. *Dalton Trans.* **2007**, 1552–1566.
- (49) De Bruin, B.; Hetterscheid, D. G. H.; Koekkoek, A. J. J.; Grutzmacher, H. *Prog. Inorg. Chem.* **2007**, *55*, 247–354.
- (50) Dzik, W. I.; van der Vlugt, J. I.; Reek, J. N. H.; de Bruin, B. *Angew. Chem., Int. Ed.* **2011**, *50*, 3356–3358.
- (51) (a) Blanchard, S.; Derat, E.; Desage-El Murr, M.; Fensterbank, L.; Malacia, M.; Mouries-Mansuy, V. *Eur. J. Inorg. Chem.* **2012**, 376–389. (b) Caulton, K. G. *Eur. J. Inorg. Chem.* **2012**, 435–443. (c) Budzelaar, P. H. M. *Eur. J. Inorg. Chem.* **2012**, 530–534.
- (52) (a) Floriani, C.; Solari, E.; Franceschi, F.; Scopelliti, R.; Belanzoni, P.; Rosi, M. *Chem.—Eur. J.* **2001**, *7*, 3052–3061. (b) Franceschi, F.; Solari, E.; Scopelliti, R.; Floriani, C. *Angew. Chem., Int. Ed.* **2000**, *39*, 1685–1687. (c) Rosi, M.; Sgamellotti, A.; Franceschi, F.; Floriani, C. *Chem.—Eur. J.* **1999**, *5*, 2914–2920. (d) Franceschi, F.; Solari, E.; Floriani, C.; Rosi, M.; Chiesi-Villa, A.; Rizzoli, C. *Chem.—Eur. J.* **1999**, *5*, 708–721. (e) Crescenzi, R.; Solari, E.; Floriani, C.; Chiesi-Villa, A.; Rizzoli, C. *J. Am. Chem. Soc.* **1999**, *121*, 1695–1706. (f) Gallo, E.; Solari, E.; Re, N.; Floriani, C.; Chiesi-Villa, A.; Rizzoli, C. *J. Am. Chem. Soc.* **1997**, *119*, 5144–5154. (g) De Angelis, S.; Solari, E.; Gallo, E.; Floriani, C.; Chiesi-Villa, A.; Rizzoli, C. *Inorg. Chem.* **1996**, *35*, 5995–6003. (h) Gambarotta, S.; Mazzanti, M.; Floriani, C.; Zehnder, M. *J. Chem. Soc., Chem. Commun.* **1984**, 1116–1118. (i) Gambarotta, S.; Floriani, C.; Chiesi-Villa, A.; Guastini, C. *J. Chem. Soc., Chem. Commun.* **1982**, 756–758.
- (53) Lu, C. C.; Bill, E.; Weyhermüller, T.; Bothe, E.; Wieghardt, K. *J. Am. Chem. Soc.* **2008**, *130*, 3181–3197.
- (54) Lu, C. C.; Weyhermüller, T.; Bill, E.; Wieghardt, K. *Inorg. Chem.* **2009**, *48*, 6055–6064.
- (55) (a) Stieber, S. C. E.; Milsmann, C.; Hoyt, J. M.; Turner, Z. R.; Finkelstein, K. D.; Wieghardt, K.; DeBeer, S.; Chirik, P. J. *Inorg. Chem.*

- 2012**, *51*, 3770–3785. (b) Russell, S. K.; Bowman, A. C.; Lobkovsky, E.; Wieghardt, K.; Chirik, P. J. *Eur. J. Inorg. Chem.* **2012**, *535*–*545*. (c) Bowman, A. C.; Milsmann, C.; Bill, E.; Lobkovsky, E.; Weyhermüller, T.; Wieghardt, K.; Chirik, P. J. *Inorg. Chem.* **2010**, *49*, 6110–6123. (d) Bowman, A. C.; Milsmann, C.; Atienza, C. C. H.; Lobkovsky, E.; Wieghardt, K.; Chirik, P. J. *J. Am. Chem. Soc.* **2010**, *132*, 1676–1684. (e) Wile, B. M.; Trovitch, R. J.; Bart, S. C.; Tondreau, A. M.; Lobkovsky, E. B.; Milsmann, C.; Bill, E.; Wieghardt, K.; Chirik, P. J. *Inorg. Chem.* **2009**, *48*, 4190–4200.
- (56) (a) Chlopek, K.; Muresan, N.; Neese, F.; Wieghardt, K. *Chem.—Eur. J.* **2007**, *13*, 8391–8403. (b) Ghosh, P.; Bill, E.; Weyhermüller, T.; Neese, F.; Wieghardt, K. *J. Am. Chem. Soc.* **2004**, *125*, 1293–1308.
- (57) Neese, F. *J. Phys. Chem. Solids* **2004**, *65*, 781–785.
- (58) (a) Hoyt, J. M.; Sylvester, K. T.; Semproni, S. P.; Chirik, P. J. *J. Am. Chem. Soc.* **2013**, *135*, 4862–4877. (b) Sylvester, K. T.; Chirik, P. J. *J. Am. Chem. Soc.* **2009**, *131*, 8772–8773. (c) Bouwkamp, M. W.; Bowman, A. C.; Lobkovsky, E.; Chirik, P. J. *J. Am. Chem. Soc.* **2006**, *128*, 13340–13341.
- (59) Russell, S. K.; Lobkovsky, E.; Chirik, P. J. *J. Am. Chem. Soc.* **2011**, *133*, 8858–8861.
- (60) Darmon, J. M.; Stieber, S. C.; Sylvester, K. L.; Fernández, I.; Lobkovsky, E.; Semproni, S. P.; Bill, E.; Wieghardt, K.; DeBeer, S.; Chirik, P. J. *J. Am. Chem. Soc.* **2012**, *134*, 17125–17137.
- (61) (a) Monfette, S.; Turner, Z. R.; Semproni, S. P.; Chirik, P. J. *J. Am. Chem. Soc.* **2012**, *134*, 4561–4564. (b) Yu, R. P.; Darmon, J. M.; Hoyt, H. M.; Margulieux, G. W.; Turner, Z.; Chirik, P. J. *ACS Catal.* **2012**, *2*, 1760–1764. (c) Trovitch, R. J.; Lobkovsky, E.; Bill, E.; Chirik, P. J. *Organometallics* **2008**, *27*, 1470–1478. (d) Bart, S. C.; Lobkovsky, E.; Chirik, P. J. *J. Am. Chem. Soc.* **2004**, *126*, 13794–13807.
- (62) (a) Tondreau, A. M.; Atienza, C. C. H. A.; Weller, K. J.; Nye, S. A.; Lewis, K. M.; Delis, J. G. P.; Chirik, P. J. *Science* **2012**, *335*, 567–570. (b) Tondreau, A. M.; Atienza, C. C. H. A.; Darmon, J. M.; Milsmann, C.; Hoyt, H. M.; Weller, K. J.; Nye, S. A.; Lewis, K. N.; Boyer, J.; Delis, J. G. P.; Lobkovsky, E.; Chirik, P. J. *Organometallics* **2012**, *31*, 4886–4893. (c) Atienza, C. C. H. A.; Tondreau, A. M.; Weller, K. J.; Lewis, K. M.; Cruse, R.; Nye, S. A.; Boyer, J. L.; Delis, J. P.; Chirik, P. J. *ACS Catal.* **2012**, *2*, 2169–2172. (d) Tondreau, A. M.; Lobkovsky, E.; Chirik, P. J. *Org. Lett.* **2008**, *10*, 2789–2792. (e) Tondreau, A. M.; Darmon, J. D.; Wile, B. M.; Floyd, S. K.; Lobkovsky, E. B.; Chirik, P. J. *Organometallics* **2009**, *28*, 3928–3940.
- (63) Karpiniec, S. S.; McGuiness, D. S.; Britovsek, G. J. P.; Patel, J. *Organometallics* **2012**, *31*, 3439–3442.
- (64) Xu, X.; Chen, Y.; Zou, G.; Sun, J. *Dalton Trans.* **2010**, *39*, 3952–3958.
- (65) (a) Olmstead, M. M.; Power, P. P.; Shoner, S. C. *Inorg. Chem.* **1991**, *30*, 2547–2551. (b) Andersen, R. A.; Faegri, K.; Green, J. C.; Haaland, A.; Lappert, M. F.; Leung, W. P.; Rypdal, K. *Inorg. Chem.* **1988**, *27*, 1782–1786.
- (66) (a) Kern, R. J. *J. Inorg. Nucl. Chem.* **1962**, *24*, 1105–1109. (b) Bradley, D. C.; Hursthouse, M. B.; Newing, C. W.; Welch, A. J. *J. Chem. Soc., Chem. Commun.* **1972**, 567–568.
- (67) (a) Bürger, H.; Wannagat, U. *Monatsh. Chem.* **1963**, *94*, 1007–1012. (b) Andersen, R. A.; Faegri, K.; Green, J. C.; Haaland, A.; Lappert, M. F.; Leung, W. P.; Rypdal, K. *Inorg. Chem.* **1988**, *27*, 1782–1786.
- (68) (a) Evans, D. F. *J. Chem. Soc.* **1959**, 2003–2005. (b) Schubert, E. M. *J. Chem. Educ.* **1992**, *69*, 62.
- (69) Carlin, R. L. *Magnetochemistry*; Springer-Verlag: Berlin; New York, 1986.
- (70) Figgis, B. N.; Hitchman, M. A. *Ligand Field Theory and Its Applications*; Wiley-VCH: New York, 2000.
- (71) Parish, R. V. *NMR, NQR, EPR, and Mössbauer Spectroscopy in Inorganic Chemistry*; Ellis Horwood: West Sussex, England, 1990.
- (72) Gütlich, P.; Bill, E.; Trautwein, A. X. *Mössbauer Spectroscopy and Transition Metal Chemistry*; Springer: New York, 2011.
- (73) Fultz, B. *Mössbauer Spectrometry*. In *Characterization of Materials*; Kaufmann, E., Ed.; John Wiley: New York, 2011.
- (74) (a) Greatrex, R.; Greenwood, N. N. *Discuss. Faraday Soc.* **1969**, *47*, 126–135. (b) Farmery, K.; Kilner, M.; Greatrex, R.; Greenwood, N. N. *J. Chem. Soc. A* **1969**, 2339–2345.
- (75) Vasudev, P.; Jones, C. H. W. *Can. J. Chem.* **1973**, *51*, 405–410.
- (76) Collins, R. L.; Pettit, R. *J. Chem. Phys.* **1963**, *39*, 3433–3436.
- (77) Dias, G. H. M.; Morigaki, M. K. *Polyhedron* **1992**, *11*, 1629–1636.
- (78) Volpe, E. C.; Wolczanski, P. T.; Darmon, J. M.; Lobkovsky, E. B. *Polyhedron* **2013**, *52*, 406–415.
- (79) (a) Lee, Y.; Mankad, N. P.; Peters, J. C. *Nat. Chem.* **2010**, *2*, 558–565. (b) Heinrich, M. P.; Gunderson, W.; Behan, R. K.; Green, M. T.; Mehn, M. P.; Betley, T. A.; Lu, C. C.; Peters, J. C. *Proc. Natl. Acad. Sci. U. S. A.* **2006**, *103*, 17107–17112.
- (80) Chlopek, K.; Bill, E.; Weyhermüller, T.; Wieghardt, K. *Inorg. Chem.* **2005**, *44*, 7087–7089.
- (81) Allen, F. H.; Kennard, O.; Watson, D. G.; Brammer, L.; Orpen, A. G.; Taylor, R. *J. Chem. Soc., Perkin Trans. 2* **1987**, S1–S19.
- (82) Sarhan, A. A. O.; Bolm, C. *Chem. Soc. Rev.* **2009**, *38*, 2730–2744.
- (83) Lo, J. C.; Yabe, Y.; Baran, P. S. *J. Am. Chem. Soc.* **2014**, *136*, 1304–1307.
- (84) (a) Bart, S. C.; Lobkovsky, E.; Bill, E.; Chirik, P. J. *J. Am. Chem. Soc.* **2006**, *128*, 5302–5303. (b) Bowman, A. C.; Milsmann, C.; Bill, E.; Turner, Z. R.; Lobkovsky, E.; DeBeer, S.; Wieghardt, K.; Chirik, P. J. *J. Am. Chem. Soc.* **2011**, *133*, 17353–17369.
- (85) (a) Parham, W. E.; Hasek, W. R. *J. Am. Chem. Soc.* **1954**, *76*, 935–936. (b) Miller, R. J.; Schechter, H. J. *J. Am. Chem. Soc.* **1978**, *100*, 7920–7927.
- (86) (a) Gunanathan, C.; Milstein, D. *Science* **2013**, *341*, 1229712. (b) Gunanathan, C.; Milstein, D. *Acc. Chem. Res.* **2011**, *44*, 588–602.
- (87) (a) Tejel, C.; del Río, M. P.; Asensio, L.; van den Bruele, F. J.; Ciriano, M. A.; Spithas, N. T. I.; Hetterscheid, D. G. H.; de Bruin, B. *Inorg. Chem.* **2011**, *50*, 7524–7534. (b) Tejel, C.; del Río, M. P.; Ciriano, M. A.; Reijerse, E. J.; Hartl, F.; Záliš, S.; Hetterscheid, D. G. H.; Spithas, N. T. I.; de Bruin, B. *Chem.—Eur. J.* **2009**, *15*, 11878–11889. (c) Tejel, C.; Ciriano, M. A.; del Río, M. P.; Hetterscheid, D. G. H.; Spithas, N. T. I.; Smits, J. M. M.; de Bruin, B. *Chem.—Eur. J.* **2009**, *14*, 10932–10936. (d) Tejel, C.; Ciriano, M. A.; del Río, M. P.; van den Bruele, F. J.; Hetterscheid, D. G. H.; Tsichlis i Spithas, N. T. I.; de Bruin, B. *J. Am. Chem. Soc.* **2008**, *130*, 5844–5845.
- (88) (a) Chang, Y.-H.; Nakajima, Y.; Tanaka, H.; Yoshizawa, K.; Ozawa, F. *Organometallics* **2014**, *33*, 715–721. (b) Chang, Y.-H.; Nakajima, Y.; Tanaka, H.; Yoshizawa, K.; Ozawa, F. *J. Am. Chem. Soc.* **2013**, *135*, 11791–11794.
- (89) (a) Rappoport, Z. *The Chemistry of Phenols*; Wiley: Chichester, U.K., 2003. (b) *Oxidative Coupling of Phenols*; Taylor, W. I., Battersby, A. R., Eds.; M. Dekker: London, 1967.
- (90) (a) Huang, Z.; Jin, L.; Feng, Y.; Peng, P.; Yi, H.; Lei, A. *Angew. Chem., Int. Ed.* **2013**, *52*, 7151–7155. (b) Kshirsagar, U. A.; Regev, C.; Parnes, R.; Pappo, D. *Org. Lett.* **2013**, *15*, 3174–3177.
- (91) Wang, K. L.; Lu, M.; Yu, A.; Zhu, X. Q.; Wang, Q. M. *J. Org. Chem.* **2009**, *74*, 935–938.
- (92) Goldstein, M.; Hoffmann, R. *J. Am. Chem. Soc.* **1971**, *93*, 6193–6204.
- (93) Zhao, Y.; Truhlar, D. G. *Acc. Chem. Res.* **2008**, *41*, 157–167.
- (94) Krishnan, R.; Binkley, J. S.; Seeger, R.; Pople, J. A. *J. Chem. Phys.* **1980**, *72*, 650–654.
- (95) Frisch, M. J.; Trucks, G. W.; Schlegel, H. B.; Scuseria, G. E.; Robb, M. A.; Cheeseman, J. R.; Scalmani, G.; Barone, V.; Mennucci, B.; Petersson, G. A.; Nakatsuji, H.; Caricato, M.; Li, X.; Hratchian, H. P.; Izmaylov, A. F.; Bloino, J.; Zheng, G.; Sonnenberg, J. L.; Hada, M.; Ehara, M.; Toyota, K.; Fukuda, R.; Hasegawa, J.; Ishida, M.; Nakajima, T.; Honda, Y.; Kitao, O.; Nakai, H.; Vreven, T.; Montgomery, J. A., Jr.; Peralta, J. E.; Ogliaro, F.; Bearpark, M.; Heyd, J. J.; Brothers, E.; Kudin, K. N.; Staroverov, V. N.; Kobayashi, R.; Normand, J.; Raghavachari, K.; Rendell, A.; Burant, J. C.; Iyengar, S. S.; Tomasi, J.; Cossi, M.; Rega, N.; Millam, J. M.; Klene, M.; Knox, J. E.; Cross, J. B.; Bakken, V.; Adamo, C.; Jaramillo, J.; Gomperts, R.; Stratmann, R. E.; Yazayev, O.; Austin, A. J.; Cammi, R.; Pomelli, C.; Ochterski, J. W.; Martin, R. L.

Morokuma, K.; Zakrzewski, V. G.; Voth, G. A.; Salvador, P.; Dannenberg, J. J.; Dapprich, S.; Daniels, A. D.; Farkas, Ö.; Foresman, J. B.; Ortiz, J. V.; Cioslowski, J.; Fox, D. J. *Gaussian 09, Revision C 01*; Gaussian, Inc.: Wallingford, CT, 2009.